Received: 2 December 2021 | Revised: 22 December 2022 | Accepted: 23 December 2022

DOI: 10.1002/esp.5539

RESEARCH ARTICLE

ESPL WILEY

Himalayan hazard cascades – modern and medieval outburst floods in Pokhara, Nepal

Melanie Fischer[1] | Karin Lehnigk[2] | Natalie Lützow[1] | Jana Brettin[1] | Georg Veh[1] | Isaac J. Larsen[2] | Oliver Korup[1,3] | Ariane Walz[1]

[1]Institute of Environmental Science and Geography, University of Potsdam, Potsdam, Germany

[2]Department of Geosciences, University of Massachusetts Amherst, Amherst, Massachusetts, USA

[3]Institute of Geosciences, University of Potsdam, Potsdam, Germany

Correspondence
Melanie Fischer, Institute of Environmental Science and Geography, University of Potsdam, Karl-Liebknecht-Straße 24-25, 14476 Potsdam, Germany.
Email: melaniefischer@uni-potsdam.de

Funding information
Deutsche Forschungsgemeinschaft, Grant/Award Numbers: 2043/2, GRK 2043/1; Deutsche Forschungsgemeinschaft (DFG); University of Potsdam; National Science Foundation

Abstract

In May 2012, a sediment-laden flood along the Seti Khola (= river) caused 72 fatalities and widespread devastation for > 40 km in Pokhara, Nepal's second largest city. The flood was the terminal phase of a hazard cascade that likely began with a major rock-slope collapse in the Annapurna Massif upstream, followed by intermittent ponding of meltwater and subsequent outburst flooding. Similar hazard cascades have been reported in other mountain belts, but peak discharges for these events have rarely been quantified. We use two hydrodynamic models to simulate the extent and geomorphic impacts of the 2012 flood and attempt to reconstruct the likely water discharge linked to even larger medieval sediment pulses. The latter are reported to have deposited several cubic kilometres of sediment in the Pokhara Valley. The process behind these sediment pulses is debated. We traced evidence of aggradation along the Seti Khola during field surveys and from RapidEye satellite images. We use two steady-state flood models, HEC-RAS and ANUGA, and high-resolution topographic data, to constrain the initial flood discharge with the lowest mismatch between observed and predicted flood extents. We explore the physically plausible range of simplified flood scenarios, from meteorological (1000 $m^3 s^{-1}$) to cataclysmic outburst floods (600,000 $m^3 s^{-1}$). We find that the 2012 flood most likely had a peak discharge of 3700 $m^3 s^{-1}$ in the upper Seti Khola and attenuated to 500 $m^3 s^{-1}$ when arriving in Pokhara city. Simulations of larger outburst floods produce extensive backwater effects in tributary valleys that match with the locations of upstream-dipping medieval-age slackwater sediments in several tributaries of the Seti Khola. Our findings are consistent with the notion that the medieval sediment pulses were linked to outburst floods with peak discharges of >50,000 $m^3 s^{-1}$, though discharge may have been an order of magnitude higher.

KEYWORDS
ANUGA, GLOF, HEC-RAS, hydrodynamic modelling, peak discharge reconstruction, RapidEye, sedimentary evidence, simulations

1 | INTRODUCTION

Unprecedented rates of contemporary atmospheric warming have spurred research on a multitude of associated geomorphic responses in high mountains (Haeberli & Whiteman, 2021; Hock et al., 2019). The recent growth in interest in cryospheric mass flows, and especially landslides, as parts of entire process cascade has offered detailed case studies that reconstruct how rapid slope failures of rock and ice impact naturally dammed lakes, cause outburst waves, and transform into long-runout debris flows (Dai et al., 2020; Jacquemart et al., 2020; Shugar et al., 2021). These cascades can have destructive consequences for settlements and infrastructure on valley floors tens

TABLE 1 Reported flood estimates of the May 2012 flood along the Seti Khola (for a comparison with this study's results also see Figure 10)

Location (see Figure 1)	Flood estimates: Peak discharge, Q_p ($m^3\ s^{-1}$)	Flood volume, V (m^3)	Reference
Kharapani village	8400	7.48×10^6	Gurung et al., 2015
	8400	8.32×10^6	Oi et al., 2012
Seti dam	>1000	2×10^6 to 10^7	Kargel et al., 2013
	935 (2.15 m water level)	–	SANDRP, 2014
Karuwa village	12300	8.32×10^6	Oi et al., 2012
Ghachok	3300	8.32×10^6	Oi et al., 2012

of kilometres beyond the source. Several recent destructive landslides have received extensive attention. For example, the 2017 Xinmo rock avalanche in China has been the focus of nearly 80 scientific papers (e.g., Fan et al., 2017; Huang et al., 2019). Other examples include the 2000 Yigong rock avalanche, south-eastern Tibetan Plateau (Shang et al., 2003); the 1987 Parraguirre rock avalanche, Chile (Hauser, 2002); the 1970 Nevados Huascaran rock avalanche, Peru (Evans et al., 2009); and the 2021 Chamoli rock-ice avalanche, India (Shugar et al., 2021). Sedimentary evidence is often used to reconstruct the magnitude and behaviour of past events (Ely & Baker, 1985; Toonen et al., 2020; Wilhelm et al., 2018). However, mass flow deposits are reworked swiftly, and limited exposure make it challenging to reconstruct past flows. Here we utilize fresh sedimentary deposits and hydrodynamic modelling to place constraints on the terminal flow phase of a recent hazard cascade in and below the Annapurna Massif in Nepal. We then reconstruct the discharge associated with older and potentially flood-derived deposits from the medieval period by linking hydrodynamic model results with preserved sedimentary evidence.

On 5 May 2012 a hyperconcentrated flow impacted the Seti Khola (= river) in the Pokhara Basin, Nepal's second most densely populated area. The flood claimed at least 72 lives and incurred a loss of some 50 million Nepalese Rupee (370,000 Euro) (Gurung et al., 2015; see Gurung et al., 2021 for a list of impacts). International media initially attributed the flood to a glacial lake outburst, whereas subsequent field and remote sensing investigations identified a series of rock-slope failures in the Annapurna Massif > 20 km upstream as the cause (Kargel et al., 2013). Field reconnaissance (e.g., Gurung et al., 2015; Kargel et al., 2013; Oi et al., 2012; SANDRP, 2014) and scientific studies (e.g., Dwivedi & Neupane, 2013; Hanisch et al., 2013) were conducted in the immediate aftermath to infer the mechanism(s) that triggered the sediment-laden flood. Debris generated by the landslides proposedly blocked the narrow and steep headwater gorge of the Seti Khola, impounding meltwater from the partly glacier-covered Sabche Cirque (Gurung et al., 2015; Kargel et al., 2013). A subsequent rock- and ice-avalanche of 33 million m^3 (Oi et al., 2014) fell from the south-western ridge of Annapurna IV (7525 m above sea level [a.s.l.]), and caused the rockslide dam to burst, although the sequence of events remains debated (Hanisch et al., 2013). The sediment-laden flood released by the proposed dam break rushed through a steep bedrock gorge in the headwaters of the Seti Khola, and destroyed Kharapani village (1100 m a.s.l.) some 18 km downstream. The flood had more than 20 reported pulses involving some estimated 7.5 million m^3 of water and sediment and a peak discharge Q_p of 8400 $m^3\ s^{-1}$ (Gurung et al., 2015; Kargel et al., 2013). There are no stream gauge data to infer discharge, hence previous studies estimated Q_p from video footage and empirical flow equations at a limited number of river cross-sections (Table 1). Sedimentation associated with the flood has also been evaluated at a limited number of locations; based on data from five cross-sections, Gurung et al. (2021) suggest there was net deposition during the May 2012 flood. We expand on these local assessments by combining hydrodynamic modelling and sedimentary evidence gathered along the length of the Seti Khola to quantify discharge and compare our values against previous estimates.

Our analysis utilizes fresh flood deposits to infer flood stage, and hence discharge, an approach that has been used to reconstruct preinstrumental and prehistoric floods (Wohl, 1995). The spatial extent of the 2012 hazard cascade is much smaller than that of at least three medieval (12th to 14th century CE) catastrophic sediment pulses that originated in the Annapurna Massif and are recorded in the valley fill of the Pokhara Basin (Fort, 2010; Schwanghart et al., 2016). These sediment pulses were likely derived from a combination of earthquake-triggered rock-ice avalanches, dam-break floods, debris flows, and intermittent fluvial reworking (Schwanghart et al., 2016; Stolle et al., 2017). However, the exact nature of the underlying depositional processes remains unclear. Although sedimentary evidence suggests an important role of fluvial processes, flow dynamics have not been evaluated quantitatively. Although a number of large prehistoric outburst events or hazard cascades are known from the Himalayas (Coxon et al., 1996; Srivastava et al., 2017; Turzewski et al., 2019), their flow characteristics are challenging to reconstruct. The Late Pleistocene (26.9 to 43.4 ka BP) outburst of former glacial lake Batal in the Lahul Himalaya, India, impacted the Chandra Valley with an estimated Q_p of 27,000 $m^3\ s^{-1}$ and a total flood volume of 1.5 km^3 (Coxon et al., 1996; Richardson & Reynolds, 2000). Based on observations of large, exotic boulders in the Trishuli and Sunkoshi Rivers of the Central Himalaya, Huber et al. (2020) suggested that mid-Holocence outbursts along these rivers had peak discharges between 10^3 and 10^5 $m^3\ s^{-1}$. Even larger Quaternary glacier- and landslide-dammed outburst floods (Q_p > 10^5 $m^3\ s^{-1}$) occurred along the Yigong River, China (Korup & Montgomery, 2008; Turzewski et al., 2019).

Here we use numerical hydrodynamic models to reconstruct flow dynamics along the Seti Khola during the 2012 flood and the proposed medieval outburst floods. Hence, we focus solely on the downstream flow phases of these hazard cascades. We pursue two objectives. First, we use a HEC-RAS model calibrated using mapped sedimentary evidence of the 2012 flood to assess whether and how well our simulations match estimates of peak discharge largely derived from eyewitness accounts and amateur video footage. Second, we use ANUGA to simulate a much higher range of peak discharges for the presumed medieval outburst floods, and determine which of these is most consistent with reported sedimentary evidence. Hence, we assess whether the medieval sedimentary record, which suggests rapid aggradation occurred, is also physically plausible, if not attributable, to outburst floods in the Pokhara Basin.

2 | STUDY AREA

The Pokhara Basin is one of several Himalayan intramontane basins that formed during the collision of the Eurasian and Indo-Australian plates, which commenced between 50 to 45 Ma. The basin is in the Pahar zone between the Higher Himalaya and the Lesser Himalaya (Mahabharat Range) (Fort, 2010). The average tectonic uplift rate near the Annapurna Massif is 7 mm yr^{-1}, partly caused by reactivation of faults running along the Main Central Thrust, which separates the Higher and Lesser Himalayan units (Burbank et al., 2003; Grandin et al., 2012). This fault zone juxtaposes the > 8-km high Annapurna Massif with the < 1-km high Pokhara Basin along one of the steepest topographic gradients in the Central Himalaya. The pre-Cenozoic bedrock is mainly sedimentary and metamorphic rocks of the Tethyan sedimentary series (TSS), the Higher-Himalaya crystalline (HHC), and the Lower Himalayan Sequence (LHS). The Seti Khola is the main river draining the Annapurna Massif to the south, where it has built a 140-km^2 fan in the Pokhara Basin. The river originates at 3700 m a.s.l. in the large Sabche Cirque (115 km^2), fed by meltwater from the Annapurna Massif, and reaches Pokhara city at 850 m a.s.l. some 35 km downstream (Figure 1).

The most recent sediment fill in the Pokhara Basin is a large alluvial fan with an estimated volume of > 1 km^3 (Blöthe & Korup, 2013) and at least three depositional units: the Tallakot, Ghachok, and Pokhara Formations (Fort, 2010; Schwanghart et al., 2016). The conglomeratic deposits of the stratigraphically oldest Tallakot and the overlying Ghachok Formations are inferred to have been deposited by Pleistocene to post-LGM (last glacial maximum) mass flows from the Sabche Cirque (Fort, 2010). The stratigraphically youngest Pokhara Formation is 60–100 m thick (Fort, 2010), with decimetre- to metre-thick cobble to boulder beds of HHC provenance (Fort, 2010; Schwanghart et al., 2016). Radiocarbon dates of the Pokhara Formation are medieval and coincide with the timing of at least three documented $M > 8$ earthquakes (1100, 1255, 1344 CE), such that the deposits may have arisen from seismically triggered, long-runout mass flows (Schwanghart et al., 2016). The processes responsible for these sediment pulses along the Seti Khola remain unclear and both lake outburst floods and long-runout ice-rock avalanches have been discussed as likely candidates (Schwanghart et al., 2016; Stolle et al., 2017). Due to this ambiguous nature (potential terminology: mass flows, debris flows, or [outburst] floods, etc.), we use the more neutral term '(medieval) sediment pulses', following the terminology of Schwanghart et al. (2016). However, as we test the plausibility of whether these sediment pulses were outburst floods representing the terminal phase of a larger hazard cascade with our models, they will also be referred to as '(medieval) outburst floods' in the context of our simulations.

The Seti Khola cuts through the Pokhara Basin fill for 70 km, having formed broad, unpaired cut-and-fill terraces > 100 m high in the

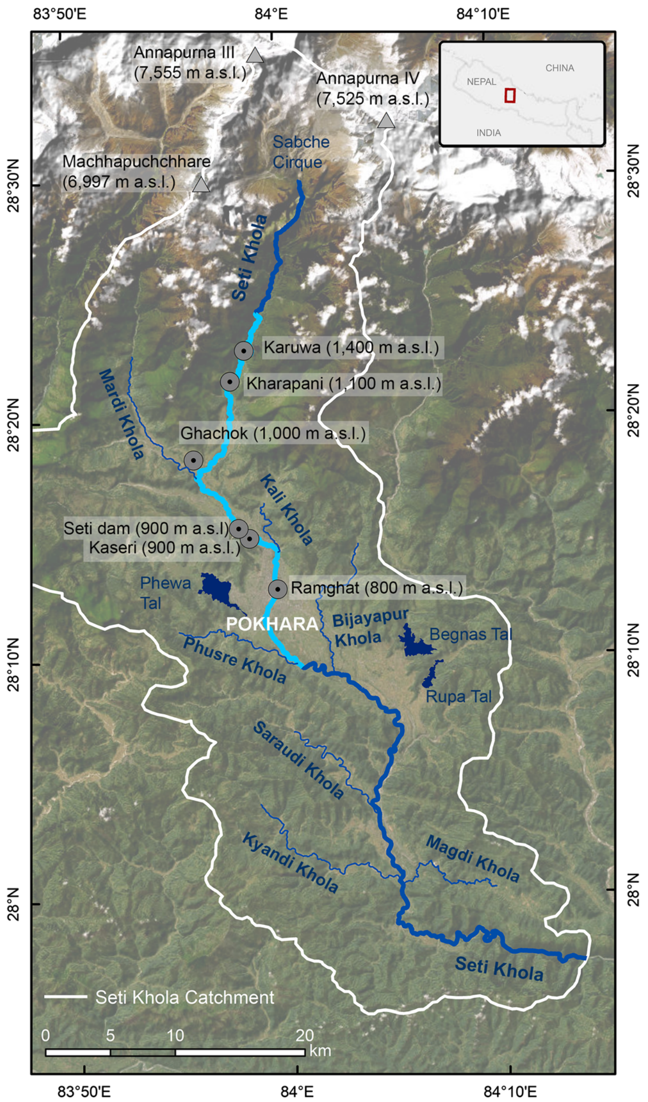

FIGURE 1 The Pokhara Valley and its main drainage system, the Seti Khola and its tributaries. We studied the light blue river reach during our field seasons in October of 2016 and 2019. Displayed on ESRI basemap Maxar satellite imagery acquired in 2020 (ESRI and Maxar Technologies, 2022). [Color figure can be viewed at wileyonlinelibrary.com]

Pokhara urban area (Fort, 2010; Hormann, 1974; Stolle et al., 2019). Several gorges less than 1 km long but up to 90 m deep occur in the indurated, calcareous Ghachok Formation and the LHS bedrock (Fort, 2010; Stolle et al., 2019). Several lakes (Phewa, Rupa, and Begnas) formed when the medieval and older mass-flow deposits of the Seti Khola dammed several tributary mouths (Fort, 2010; Stolle et al., 2019).

The climate is seasonal with heavy summer monsoon rainfall on the southern flank of the Annapurna Massif from May to October, when > 80% of the mean annual precipitation of 4000 mm occurs (Ross & Gilbert, 1999). The central Pokhara Basin has a humid subtropical to humid temperate climate with mean monthly temperatures of 12.8 to 25.8°C (Ross & Gilbert, 1999), whereas the Annapurna Massif has temperate to alpine climate.

Pokhara is Nepal's second largest city with an estimated population of 523,000 in 2020 that tripled since the 1990s (Rimal et al., 2015). In past decades, the city and the surrounding basin have seen rapid growth in population and tourism. Urban areas increased by 30 km^2 between 1990 and 2013. Migration caused a 45% increase of urban areas from 1977 to 2010 (Rimal, 2012; Rimal et al., 2015). Urbanization also led to an increase in construction of informal settlements along the active channel of the Seti Khola (Rimal et al., 2015, 2018).

3 | METHODS

3.1 | Data and data acquisition

The hydrodynamic simulations routed flow over a pre-processed 5-m ALOS WORLD digital elevation model (AW3D DEM) of the Seti Khola catchment, which is derived from a mosaic of ALOS stereo-imagery acquired between 2006 and 2011. The vertical datum of the DEM is the EGM96 geoid, and the projection is UTM Zone 44 N. We surveyed 93 cross-sections along a 30-km long stretch of the Seti Khola and its terraces from near Karuwa village (1550 m a.s.l.) to the Phusre Khola confluence in the southern outskirts of Pokhara (646 m a.s.l.) with a TruPulse 360 laser range finder and a Garmin eTrex handheld global positioning system (GPS) in October 2016 and October 2019. We used our field data to manually correct the DEM-derived cross-sections along the Seti Khola's deep and narrow gorges as the resolution of the AW3D DEM was not able to accurately capture the topography there.

We estimated Manning's *n*, that is a hydraulic loss coefficient, for the channel at 61 field sites following the method of Arcement & Schneider (1984) and Chow (1959). For the floodplains, we linked Manning's *n* to land-cover types that we manually mapped from a 1-m resolution Maxar satellite image from 2020 that is available as ESRI basemap (ESRI and Maxar Technologies, 2022). We used land-cover classes by the United States Geological Survey (USGS) National Land Cover Database to estimate Manning's *n* values following recommendations by Brunner (2020b) (Figure 2). Manning's *n* is a major source of uncertainty in numerical hydraulic models (Brunner, 2020a; Klimeš et al., 2014) and we conducted a sensitivity analysis to estimate this uncertainty.

Reported flood stages for the 2012 flood are limited to the Seti dam (SANDRP, 2014). Hence, we mapped flood deposits as indicators for peak flow stage, following the methods that Wohl (1995) used to reconstruct glacial lake outburst floods (GLOFs) in eastern Nepal. We mapped flood deposits and inundation limits of the 2012 outburst from an orthorectified 5-m resolution RapidEye satellite image acquired on 18 October 2012, which was the first cloud-free image following the flood (Planet Team, 2017). Flood sediments stood out as bright pixels on otherwise dark green, vegetated terraces. Mapped extents of upstream-dipping slackwater deposits located up to several kilometres upstream of tributary junctions served as approximate markers of medieval sediment pulses (Fort, 2010; Stolle et al., 2019). These markers may have been subject to subsequent erosion, and hence delineate the minimum extent of deposition.

3.2 | Numerical flood routing with HEC-RAS

Studies of Himalayan outburst floods increasingly use numerical hydrodynamic models to simulate flood routing (Westoby et al., 2014; Worni et al., 2014; Zhang & Liu, 2015). These models are based on the conservation of mass and momentum and solved for channels and floodplains with known geometry and surface roughness (Westoby et al., 2014; Worni et al., 2014; Zhang & Liu, 2015). Among the many models developed to simulate geophysical flows (e.g., BASEMENT by Faeh et al., 2011, DAMBRK by Fread, 1988, Flo-2D by O'Brien et al., 1993, D-Claw by George et al., 2017 and r.avaflow by Mergili et al., 2017), we used HEC-RAS, which has been widely adopted for simulating outburst floods (Cenderelli & Wohl, 2003; Klimeš et al., 2014; Sattar et al., 2021; Wang et al., 2012), to simulate the terminal flow phase of the 2012 hazard cascade.

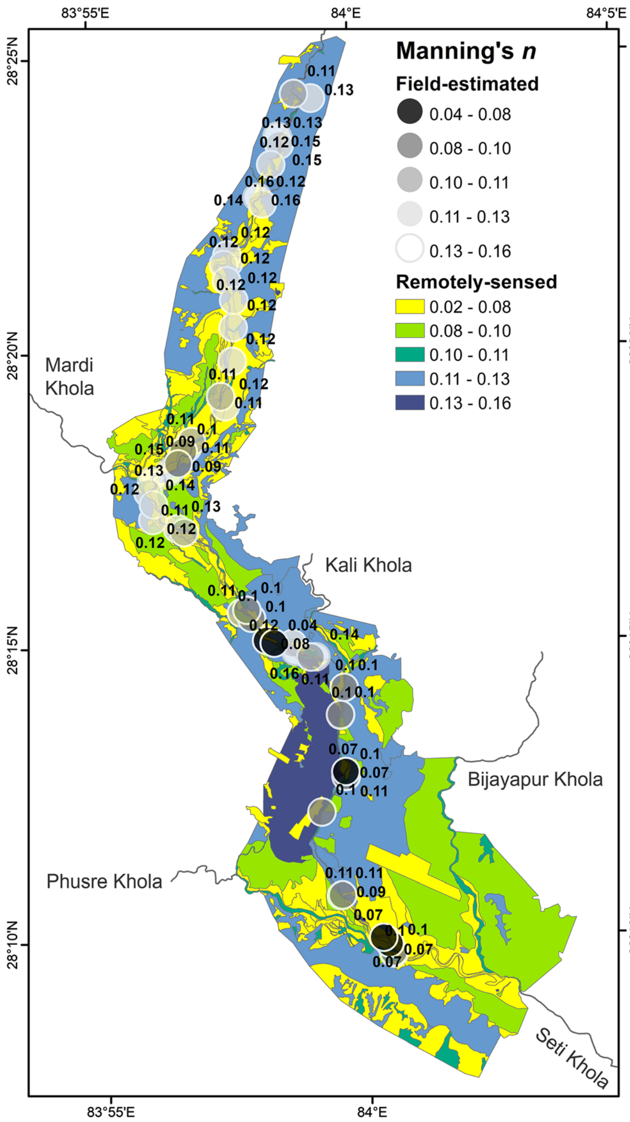

FIGURE 2 Manning's *n* values estimated in the field (or from field-photographs) with the Arcement and Schneider (1984) method (grey circles) and as remotely-sensed land cover class mapping (coloured polygons) from ESRI basemap Maxar satellite imagery acquired in 2020 (ESRI and Maxar Technologies, 2022). [Color figure can be viewed at wileyonlinelibrary.com]

Numerical hydrodynamic modelling of water flowing in open channels is based on the hydraulic principles described by the shallow water equations or, for one-dimensional (1D) flow, by the Saint-Venant equation (Westoby et al., 2014; Worni et al., 2014; Zhang & Liu, 2015). We used HEC-RAS version 5.0.7 (https://www.hec.usace.army.mil/software/hec-ras/), which applies a step method for simulating 1D steady, that is gradually varied but constant, channel flow

(Brunner, 2020a; Klimeš et al., 2014). We followed the recommendations by Brunner (2020b) and choose HEC-RAS 1D modelling over the computationally more expensive two-dimensional (2D) modelling as the May 2012 flood along the steep Seti Khola was highly gravity driven and flow generally followed the river's path. In 1D form, HEC-RAS computes water surface profiles by iteratively solving Equation (1), in which flow energy losses are due to friction, contraction, and expansion in the natural channel geometry (Brunner, 2020a):

$$Z_2+Y_2+\frac{a_2V_2^2}{2g}=Z_1+Y_1+\frac{a_1V_1^2}{2g}+h_e, \quad (1)$$

where Z_1 and Z_2 are the elevations of the main channel bed at cross-sections 1 and 2, Y_1 and Y_2 are the corresponding flow depths, V_1 and V_2 are the mean flow velocities, and a_1 and a_2 are weighting coefficients; g is the gravitational acceleration and h_e is the energy head loss (Equation 2):

$$h_e=L\bar{S}_f+C\left|\frac{a_2V_2^2}{2g}-\frac{a_1V_1^2}{2g}\right|, \quad (2)$$

where L is the distance weighted reach length, $\bar{S}_f$ is the energy gradient, and C is the expansion (or contraction) loss coefficient. The discharge Q for each cross-section is calculated using Manning's equation (Equation 3):

$$Q=\frac{1}{n}AR^{2/3}S_f^{1/2}, \quad (3)$$

where A is the cross-sectional area of the flow and R is the hydraulic radius.

HEC-RAS allows for modelling steady flow in subcritical, supercritical, or mixed flow regimes (Brunner, 2020a). For modelling supercritical flow in HEC-RAS, the necessary critical depth for each cross-section is iteratively solved via the total energy head H (Equation 4):

$$H=WS+\frac{aV^2}{2g}, \quad (4)$$

where WS is the water surface elevation and $\frac{aV^2}{2g}$ is the velocity head.

We computed water-surface-profiles in HEC-RAS for a total of 572 cross-sections at roughly 90-m spacing for the main reach of the Seti Khola and three major tributaries (Mardi, Kali, and Phusre Khola) (Figure 3). We also assigned our land-cover- and field-based estimates of Manning's n values to the channel and overbank portions of each cross-section.

Both video footage and previous peak discharge estimates of the 2012 flood (Table 1) focus on the heavily impacted uppermost reach of the Seti Khola, between Ghachok and Karuwa and especially at Kharapani, as well as Pokhara's north-western urban periphery, where the informal settlement of Kaseri is situated just a few hundred metres downstream of the Seti dam (Figure 1). As the only recorded flood stage of the event was measured at this dam, we decided to reconstruct flow behaviour in a detailed model within this area, utilizing a sub-section of the model domain consisting of 29 cross-sections.

We first simulated previous estimates of peak discharge (Table 1) with HEC-RAS. We simulate a Q_p of 8400 m^3 s^{-1} in the in the upper

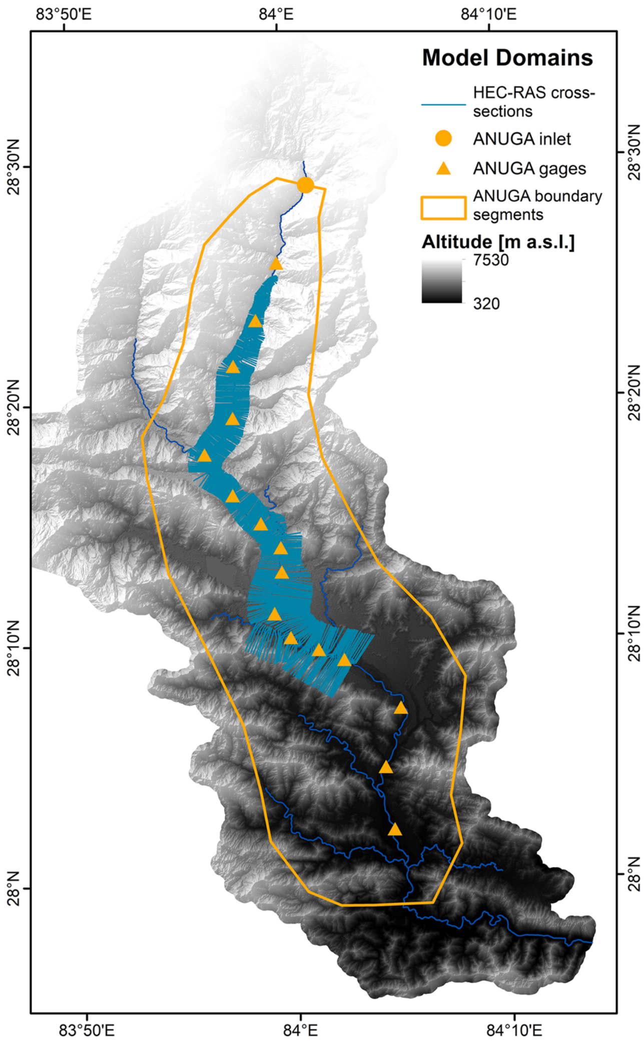

FIGURE 3 Spatial extents of the HEC-RAS and ANUGA model domains and the topography derived from the 5-m ALOS DEM (©NTT DATA, RESTEC/included©JAXA). Note that although depicted as point, the ANUGA inlet is defined as reflective boundary segment. [Color figure can be viewed at wileyonlinelibrary.com]

Seti Khola reach, which is based on estimates for Kharapani from Gurung et al. (2015) and Oi et al. (2014). Further downstream, we used the detailed model at Seti dam to test the flood reconstructions from SANDRP (2014), including the measured flood stage of 2.5 m and Q_p of 935 m^3 s^{-1}.

We then iteratively simulated Q_p values between 1000 and 10,000 m^3 s^{-1}. We approximated local Q_p during the May 2012 flood by determining which of the 29 modelled discharges produced flood inundation and stage that best matched the mapped flood inundation and field evidence of high water.

For all simulations, we distinguished between areas where predictions underestimated or overestimated the observed extent of sediment deposition. We assumed a mixed flow regime with critical flow depth as an upper boundary condition and normal depth with an approximated energy slope of 0.0065 as a lower boundary condition, given the high channel gradient and frequent alterations in channel geometry (Klimeš et al., 2014). In the detailed model at Seti dam and Kaseri, however, we replaced critical flow depth by the recorded water level as an upper boundary condition, while maintaining all other model specifications. Discharge data are unavailable, thus we

TABLE 2 Simulated peak discharge (Q_p) scenarios ($m^3\ s^{-1}$) for HEC-RAS and ANUGA and reported values in prior empirical assessments in the Pokhara Valley and case studies of comparable Himalayan hazard cascades

Q_p scenario	HEC-RAS	ANUGA	Empirically estimated Q_p ranges in prior studies	Q_p ranges of comparable Himalayan hazard cascades
1000	✓		1–12.3 × 10^3 2012 Seti Khola (Gurung et al., 2015; Kargel et al., 2013;Oi et al., 2012; SANDRP, 2014)	1.6 × 10^3 1985 Dig Tsho glacial lake outburst flood (Vuichard & Zimmermann, 1987)
2000	✓			
3000	✓			
4000	✓			
5000	✓	✓		
6000	✓			
7000	✓			
8000	✓			8–14 × 10^3 2021 Chamoli (Shugar et al., 2021)
9000	✓			
10000	✓	✓		
50000		✓	50–600 × 10^3 Medieval Pokhara sediment pulses Schwanghart et al. (2016)	61–173 × 10^3 2000 Yigong outburst flood (Turzewski et al., 2019)
100000		✓		
200000		✓		
300000		✓		
400000		✓		
500000		✓		
600000		✓		

assumed an approximated steady base flow of 100 $m^3\ s^{-1}$ (i.e., < 10% of our Q_p scenarios) in the tributaries for all scenarios.

3.3 | Numerical flood routing with ANUGA

For simulating the larger medieval outburst floods we used ANUGA, which has been used to simulate outburst floods from breaches of man-made (Mungkasi et al., 2013) and natural dams (David et al., 2022; Larsen & Lamb, 2016; Lehnigk & Larsen, 2022) and meteorological floods (Chen et al., 2021). We chose ANUGA over HEC-RAS for computational efficiency when simulating higher magnitude flows. The purpose of these simulations is to determine the smallest discharge that inundates slackwater deposits, rather than to simulate a flood hydrograph. ANUGA is a 2D, finite-volume hydrodynamic modelling software that solves the depth-averaged shallow water equations (Roberts et al., 2015). For our simulations in ANUGA, we used a triangular computational mesh generated from the 5-m ALOS DEM with a default maximum triangle area of 2500 m^2 throughout the domain (Figure 3). A smaller maximum triangle area of 50 m^2 was specified surrounding six features of interest, including a relict landslide dam and the Karuwa and Kharapani villages in the upper reach, Seti dam, Ramghat, and the Phusre confluence. The node locations in the computational mesh were automatically generated by ANUGA, with higher node density in areas with higher relief. All boundary segments were modelled as Dirichlet boundaries at which flow was permitted to exit the domain, except for the inlet which was assigned a reflective boundary condition. Grids of flow depth and stage were interpolated from the computational mesh at 5-m cell resolution for model time steps of interest. All simulations used a spatially uniform Manning's roughness coefficient of 0.091, based on our Manning's *n* estimates. Schwanghart et al. (2016) estimated a maximum discharge of 600,000 $m^3\ s^{-1}$ for the proposed medieval outburst floods based on the geometry of Sabche Cirque and three relict landslide dams in the upper Seti Khola gorge; discrete discharges up to this maximum were simulated in increments of up to 100,000 $m^3\ s^{-1}$ using a stair-step hydrograph (Table 2). Each discharge was maintained for a model run time of 150,000 s (41.67 h), which was sufficient time for flow to reach steady state as indicated by constant stage at multiple points throughout the domain; results were saved every 10,000 s (2.78 h).

3.4 | Discharge constraints from modelling and field evidence

Several aspects of our approach and the inherent assumptions might put constraints on the flood reconstructions. For example, the results of both models are sensitive to the choice of Manning's *n* (Westoby et al., 2014; Wohl, 1998). To assess the impact of Manning's *n* on our HEC-RAS simulations, we compared inundation areas and depths between models with both spatially varying and uniform Manning's $n = 0.1$ for a mixed flow for the scenario with the highest $Q_p = 10{,}000\ m^3\ s^{-1}$. This roughness value has been used in steep gravel-bed rivers (Cenderelli & Wohl, 2001). We also estimated the sensitivity of 1D flow simulations in HEC-RAS with respect to contributions from tributaries (Mardi, Kali, and Phusre Khola) compared to a model run for the Seti Khola without any tributaries.

We used the spatial extent and elevation of the Pokhara Formation in tributary valleys to estimate the Q_p of the medieval outburst floods. The field evidence for flooding included slackwater deposits mapped by Stolle et al. (2017) and two outcrops of mainly breccious conglomerates we examined near the Mardi and Phusre confluences. We computed the horizontal distance between mapped slackwater deposits and simulated flood extents for $Q_p > 50{,}000\ m^3\ s^{-1}$. We assume that the discharge that emplaced the deposits was associated with the simulated flood that resulted in the minimum mean horizontal distance. This analysis provides conservative estimates of flood size, as the elevation of slackwater deposits in the tributary valleys place minimum constraints on flood stage due to potential erosion of the fan deposits after the Pokhara Formation had been emplaced.

The topography of the Pokhara Basin prior to the catastrophic infill is unknown, but was dominated by an older, potentially less dissected alluvial fan of Ghachok Formation material (Fort, 1987). In order to test the sensitivity of our simulations of possible medieval outburst floods with respect to the currently dissected topography, we performed ANUGA modelling with the specifications described in Section 3.3 but routed flow across a smoothed, that is undissected, valley floor. To create the latter, we manipulated the ALOS DEM by filling the modern channel network on the fan to its surface (see Supporting Information Figure S1). Thus, we locally increased the valley floor elevation in a spatially non-uniform way. We used this smoothed surface as an end-member approximation of a freshly deposited fan without any incision.

4 | RESULTS

4.1 | Reconstruction of the May 2012 outburst flood

The 2012 outburst flow deposited 1.4 km^2 of sediment outside of the active channel areas (Figures 4a–c and 5a–c). Most aggradation, lateral channel migration of up to 100 m, and meander cutoffs occurred upstream of the Mardi Khola. Only at Ramghat in Pokhara city did the channel migrate laterally by some 145 m. The average lateral channel shift was 14 m, which is ~22% of the mean pre-flood channel width of 63 m. The active channel of the Seti Khola had an area of 4.0 km^2 in March and 5.1 km^2 in October 2012, with a net gain of 1.1 km^2 or an increase of 28% over a 55-km long river reach. The increase in active channel area is greater than the channel change response to annual monsoonal floods, which caused a net loss of 0.15 km^2 (4%) in the previous year (RapidEye images from 2 February 2011 to 22 March 2012; Planet Team, 2017).

Gurung et al. (2015) estimated a peak discharge of 8400 $m^3\ s^{-1}$ at Kharapani. Our simulation for this discharge at this location had a maximum inundation depth of 22 m and flow velocities of 3 $m\ s^{-1}$ to 14 $m\ s^{-1}$ (Figure 4d). Compared to local flood sediments mapped along this reach, this simulation overestimates the inundation area by 16%. SANDRP (2014) estimated a Q_p of 935 $m^3\ s^{-1}$ for a measured flow depth of 2.15 m at Seti dam. We used this information as steady flow input with the water level as an upper boundary

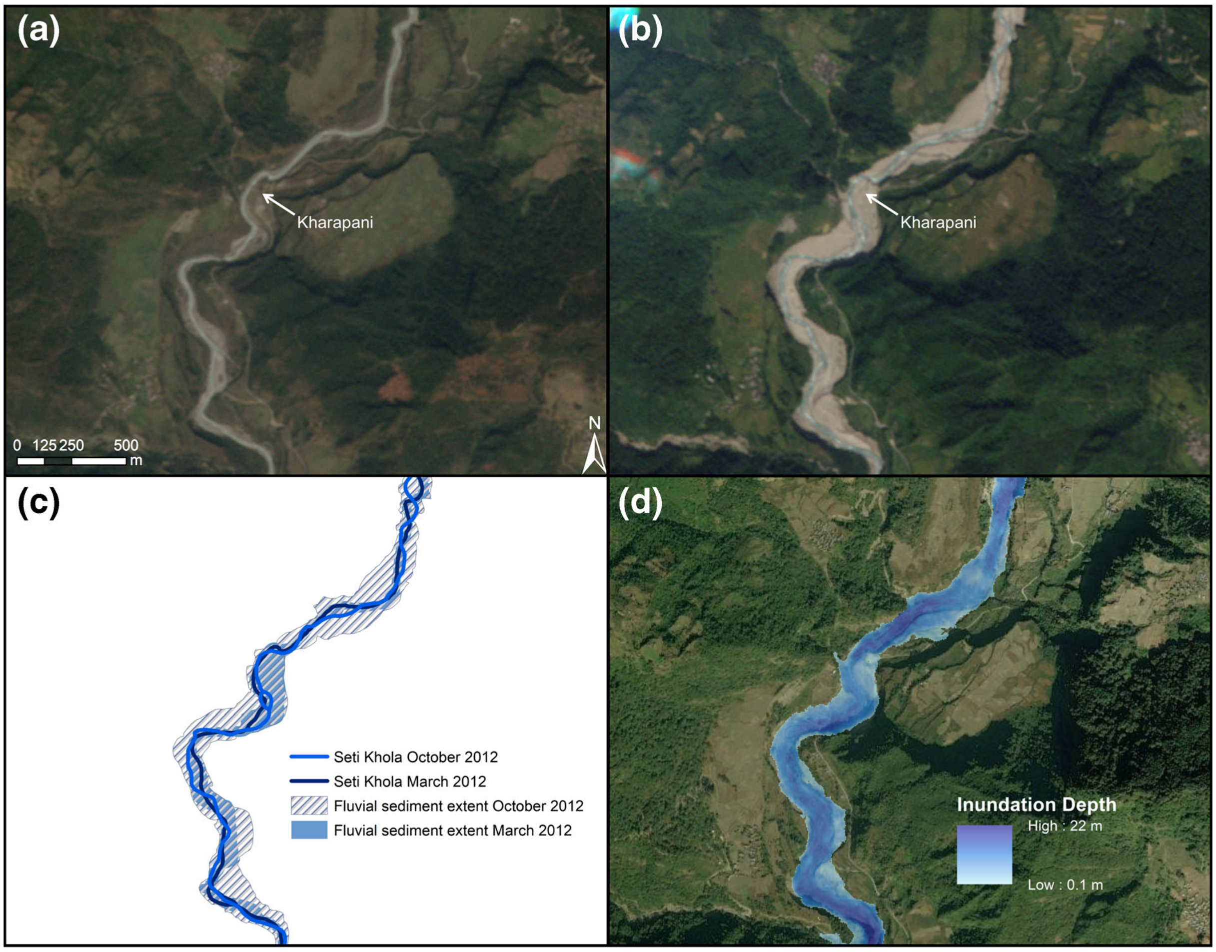

FIGURE 4 Geomorphic and simulated flood impacts at Kharapani (see Figure 1 for location). Comparison of RapidEye scenes acquired before (22 March 2012, a) and after (18 October 2012, b) the May 2012 flood (Planet Team, 2017). (c) Inundation extents and pre- and post-event course of the Seti Khola mapped from satellite imagery in (a) and (b). HEC-RAS simulated inundation depths when modelling $Q_p = 8400\ m^3\ s^{-1}$ in steady state (d), displayed on ESRI basemap Maxar satellite imagery acquired in 2020 (ESRI and Maxar Technologies, 2022). [Color figure can be viewed at wileyonlinelibrary.com]

condition in a mixed and a supercritical flow simulation (Figure 5d). Under mixed flow conditions, the overestimate between local simulated inundation and mapped flood-sediment extent is 257%. When assuming supercritical flow at Seti dam, however, modelled flood areas overestimate the mapped flood areas by 36%. Our simulation of mixed flow with 935 $m^3\ s^{-1}$ at the Seti dam has a maximum flow depth of 39 m and a flow velocity of 3.7 $m\ s^{-1}$. For supercritical conditions, the maximum inundation depth is 28 m and flow velocities range between 0.3 $m\ s^{-1}$ and 8.5 $m\ s^{-1}$. Both scenarios apply to a reach directly upstream of a narrow gorge and, hence, a reach of abrupt confinement.

When iteratively assessing the most likely initial Q_p upstream of the Mardi Khola, we find the smallest mismatch between mapped and simulated flood extents for $Q_p = 3700\ m^3\ s^{-1}$ (Figure 6a). In this scenario, the maximum flow depth along this uppermost reach is 45 m and the maximum steady-flow velocity is 28 $m\ s^{-1}$. We obtained flow depths > 22 m just upstream from a relict, breached landslide dam 2.7 km north of Karuwa village. At Kharapani, we model a maximum flow depth of 15 m and velocity that ranged from 3 $m\ s^{-1}$ to 10 $m\ s^{-1}$.

At the Seti dam, our detailed model predicts supercritical flow of 500 $m^3\ s^{-1}$ and flow velocities of 0.2–6.7 $m\ s^{-1}$ (Figure 6b).

4.2 | Simulation of medieval outburst flooding

Flow depths and inundation limits of smaller Q_p scenarios (5000 and 10,000 $m^3\ s^{-1}$) modelled with ANUGA are largely consistent with those modelled by HEC-RAS. All ANUGA outburst flood scenarios consistently simulate highest flow depths in the proximal and distal parts of the Pokhara Basin, whereas modelled flow is less confined in the central parts of the basin (Figure 7). The entire fan surface is inundated by simulated floods with $Q_p > 200{,}000\ m^3\ s^{-1}$. The ANUGA simulations predict that backwaters extend several kilometres up the main tributaries such as the Mardi and Phusre Khola for $Q_p > 50{,}000\ m^3\ s^{-1}$ (Figures 7 and 8). For simulated $Q_p > 200{,}000\ m^3\ s^{-1}$, backwater flooding extends > 8 km up the Kyandi and Magdi Khola tributaries, which are about 65 km downstream from the flood source below the Sabche Cirque. When the simulated Q_p is 600,000 $m^3\ s^{-1}$, backwater effects produce mean flow depths of 10 to 20 m at the Mardi, Kali, and Phusre Khola tributaries, and predicted mean depths of 44 m in the southern part of our study area at the Kyandi and Magdi Khola confluence. The maximum simulated flow depths for Q_p of 600,000 $m^3\ s^{-1}$ are up to 200 m in the reaches upstream of the Mardi Khola. When comparing our simulated flood extents along tributary valleys with slackwater deposit outcrops

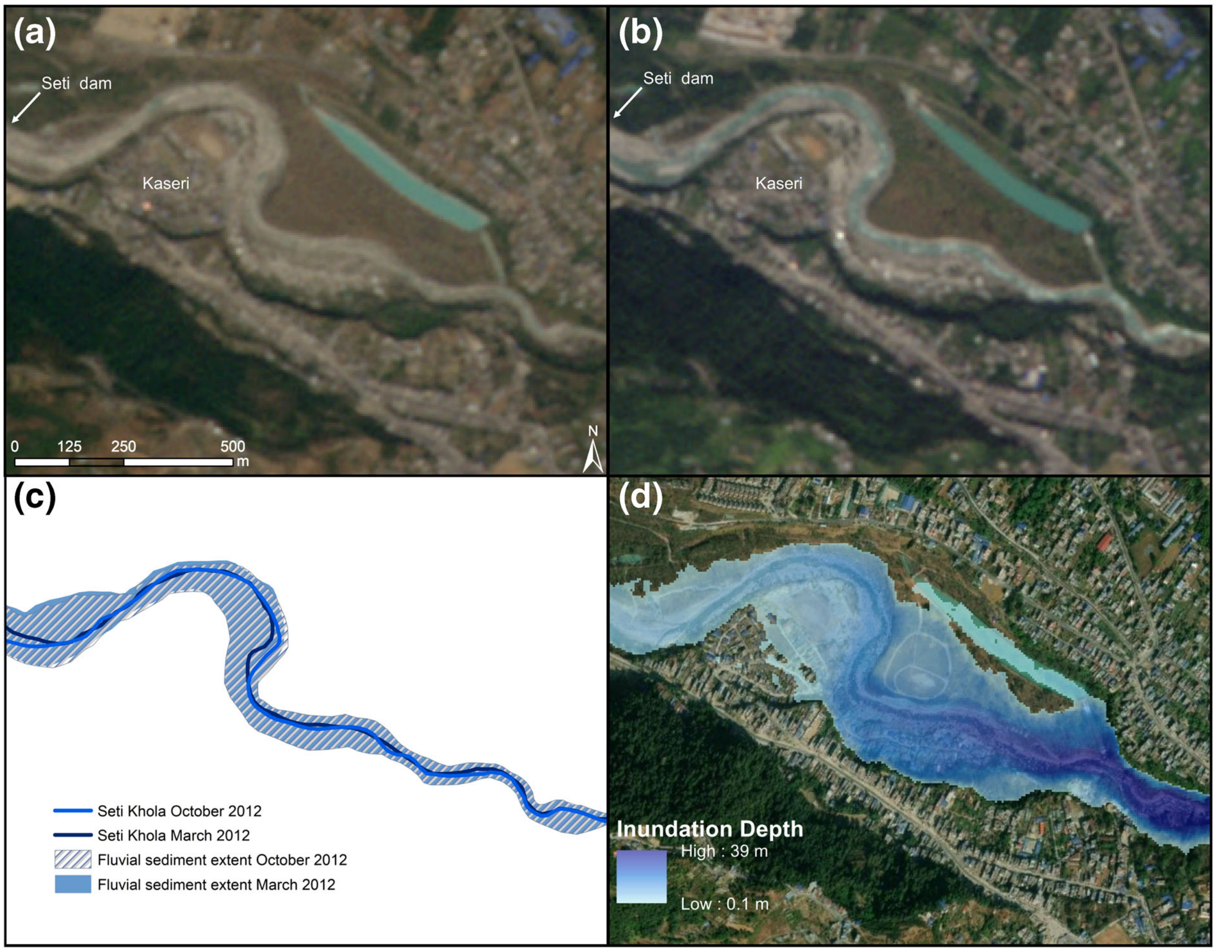

FIGURE 5 Geomorphic and simulated flood impacts at the Seti dam and Kaseri informal settlement just downstream (see Figure 1 for location). Comparison of RapidEye scenes acquired before (22 March 2012, a) and after (18 October 2012, b) the May 2012 flood (Planet Team, 2017). (c) Inundation extents and pre- and post-event course of the Seti Khola mapped from satellite imagery in (a) and (b). HEC-RAS simulated inundation depths when modelling $Q_p = 935$ m^3 s^{-1} in steady state (d), displayed on ESRI basemap Maxar satellite imagery acquired in 2020 (ESRI and Maxar Technologies, 2022). [Color figure can be viewed at wileyonlinelibrary.com]

FIGURE 6 Areas of difference (green) between the simulated inundation boundaries and the mapped flood sediment extents from RapidEye imagery in the upper reach (a) and at Seti dam (b). These are further differentiated in overestimates (blue) and underestimates (orange). In the upper reach, minimum total difference area (622,800 m^2) is achieved when simulating a Q_p of 3700 m^3 s^{-1} as upper steady flow condition. At the Seti dam, minimum total difference area (78,960 m^2) is achieved when simulating a Q_p of 500 m^3 s^{-1} and a water level of 2.5 m as the upper flow condition. [Color figure can be viewed at wileyonlinelibrary.com]

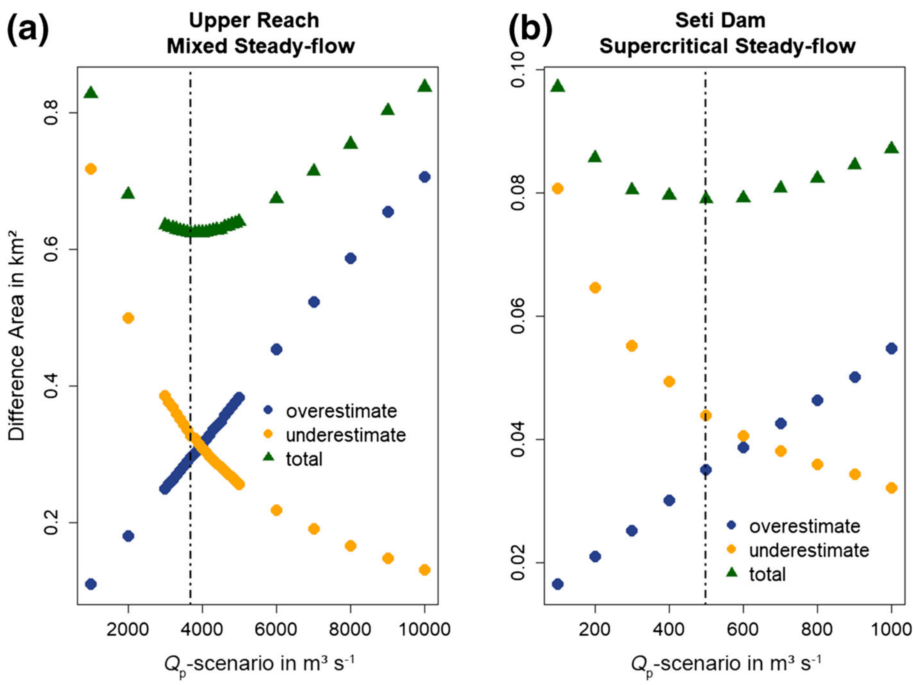

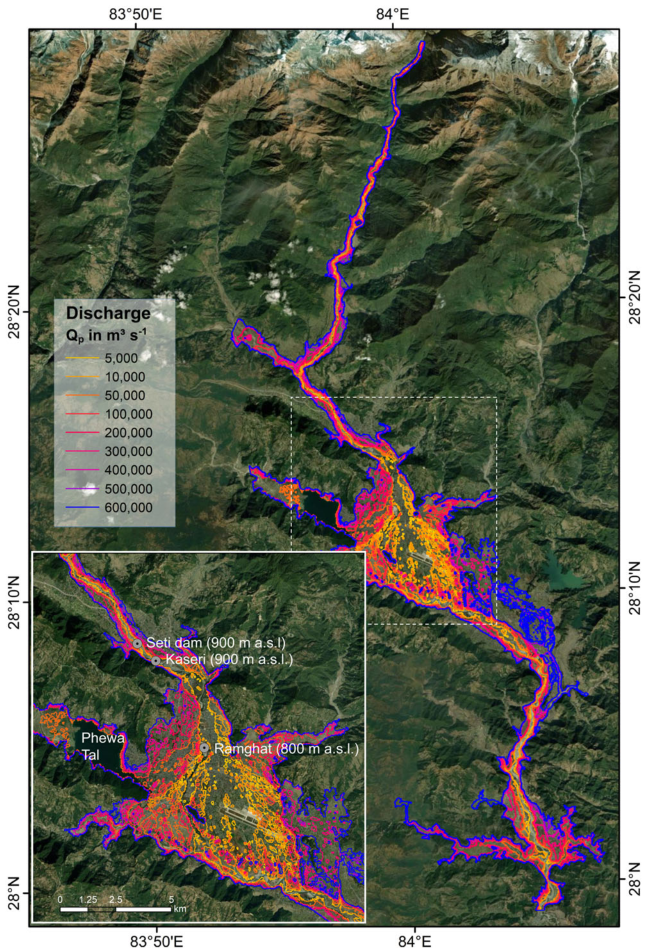

FIGURE 7 Maximum inundation limits when modelling Q_p ranging from 5000 $m^3\ s^{-1}$ to 600,000 $m^3\ s^{-1}$ in ANUGA. Note extensive simulated backwater flooding in tributary valleys for discharges > 100,000 $m^3\ s^{-1}$. Displayed on ESRI basemap Maxar satellite imagery acquired in 2020 (ESRI and Maxar Technologies, 2022). [Color figure can be viewed at wileyonlinelibrary.com]

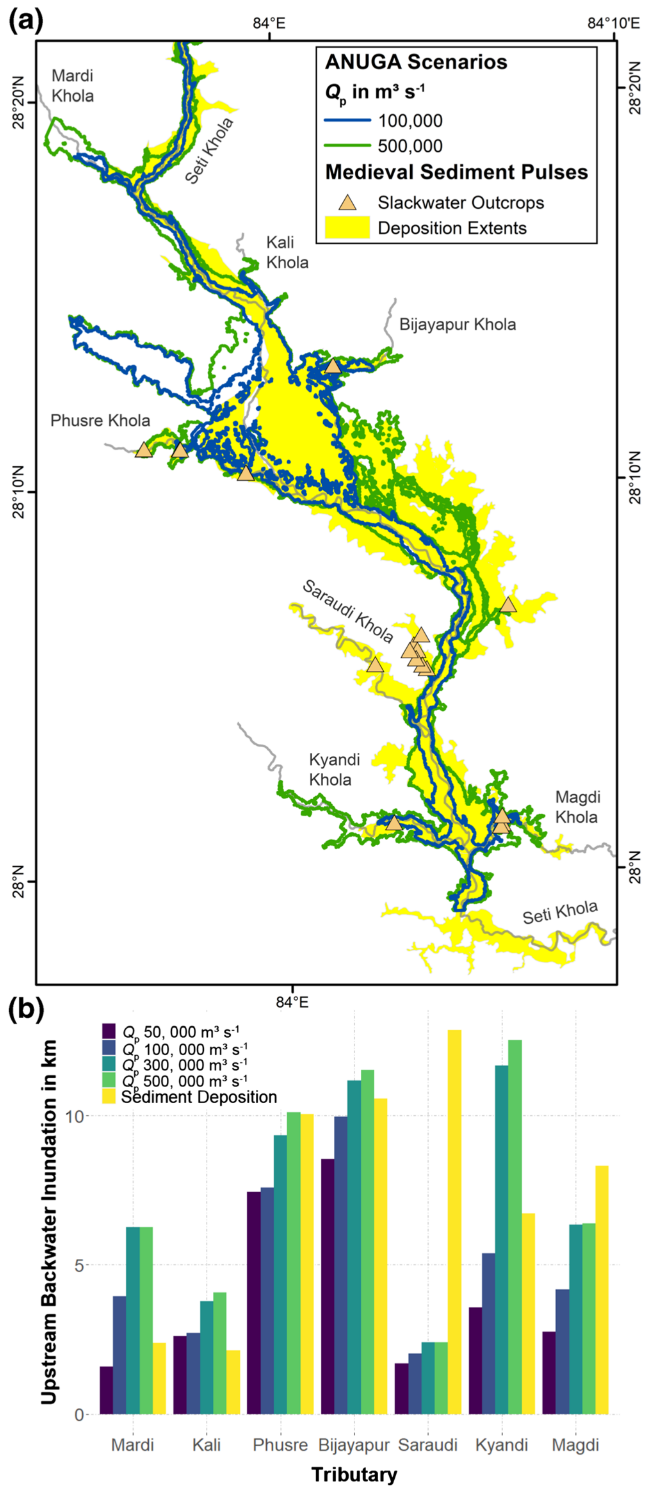

FIGURE 8 Comparison of selected maximum inundation limits of ANUGA outburst flood scenarios with sedimentary evidence of the catastrophic medieval sediment pulses (1100 to 1344 CE; Schwanghart et al., 2016; Stolle et al., 2017; data courtesy of A. Stolle). (a) Map of simulated flood limits for Q_p = 100,000 and 500,000 $m^3\ s^{-1}$ and medieval sediments across the Pokhara Basin; (b) comparison of upstream backwater inundation in major tributaries as predicted by selected Q_p scenarios and as evident in the sediment fill. [Color figure can be viewed at wileyonlinelibrary.com]

described by Stolle et al. (2017), we find that they fit best with inundation limits linked to a Q_p of 500,000 $m^3\ s^{-1}$ (Figure 8).

When simulating flow across an undissected fan surface, we found that flow dispersion across the central part of the valley is more pronounced while the fan surface is inundated for Q_p > 200,000 $m^3\ s^{-1}$. These tests of sensitivity to topography again highlight extensive simulated backwater effects in the Seti Khola's major tributaries, which commence in the Mardi, Phusre, Kyandi, and Magdi Khola for Q_p > 50,000 $m^3\ s^{-1}$ and match sedimentary evidence best again for the scenario of $Q_p = 500{,}000\ m^3\ s^{-1}$.

5 | DISCUSSION

5.1 | Model applicability

The resolution and quality of our topographic data affect to first order the accuracy of our hydraulic models. The 5-m ALOS DEM appears suitable for HEC-RAS modelling of outburst floods (Westoby et al., 2014; Zhang & Liu, 2015), but only partly resolves the steep gorges along the Seti Khola fan. Earlier attempts at field surveys with terrestrial laser scanning were hampered by haze and water vapour, while airborne mapping using unmanned aerial vehicles (UAVs) is legally restricted in Nepal. Hence, we found that a handheld laser rangefinder proved most useful and economic during field work. While our topographic data are more detailed than in most previous lake-outburst studies (e.g., Mergili et al., 2011; Somos-Valenzuela et al., 2014; Wang et al., 2018), the DEM does not reflect the topography of the Pokhara Basin at the time of the medieval sediment pulses. Hence, volumetric estimates are limited, which is a common issue in reconstructing outburst floods (Westoby et al., 2014).

There are several simplifying assumptions inherent to our modelling approach that may influence the interpretation of the results. The sedimentary record of both the May 2012 flood and the medieval sediment pulses indicates that they were likely sediment-laden and transient flows with high erosive potential. However, steady-flow models in HEC-RAS (version 5.0.7) and ANUGA both simulate clear-water flow in stable channels and, hence, ignore potential geomorphic effects during large floods such as changing topography by scouring and deposition (David et al., 2022; Larsen & Lamb, 2016; Lehnigk & Larsen, 2022) or an increase in fluid viscosity due to entrainment of sediments (Mungkasi et al., 2013). The latter might also alter flow mobility and runout (Westoby et al., 2014). The entrainment of high volumes of sediment by outburst floods increases flow volumes (Frank et al., 2015; Westoby et al., 2014). Thus, when using paleostage indicators for event reconstructions, clear-water models might overestimate both peak discharge and the volume of flood water. Further, hazard assessments relying on clear-water models might significantly underestimate the downstream impacts for outbursts of smaller bodies of water, whose momentum, peak flow duration, and flow depth might significantly increase downstream, depending on the amount of sediments available for entrainment (Carrivick, 2010; Frank et al., 2015). However, direct observations and data on the studied events are few, and based on proxies, particularly with regard to the medieval sediment pulses. To find a compromise between uncertainty and simplicity for our preliminary reconstructions we opted for clear-water models, as much of the former channel and floodplain topography remains unknown. Moreover, we believe that our choice is adequate for a first numerical test of whether outburst floods – instead of long-runout rock-ice avalanches (Schwanghart et al., 2016) – could have produced the geomorphic and sedimentary evidence of medieval sediment pulses at all. Models such as Flo-2D and the 'Mud and Debris Flow' module in HEC-RAS version 6.0 can simulate non-Newtonian flows but require rheological input parameters (Cesca & D'Agostino, 2008; Zhang & Liu, 2015) that remain unknown at the scale of our study. Due to a similar lack of information regarding initial outburst flood generation, we considered only steady flow. The Seti Khola was ungauged during the May 2012 flood, so that assuming a simple triangular hydrograph as the necessary upper boundary condition for unsteady flow models would only add more uncertainty. Moreover, empirical equations for input hydrographs are mostly site-specific (Dussaillant et al., 2010; Walder & Costa, 1996) and need additional estimates such as the breach rate and depths or potential water volumes impounded by dams in the headwaters of the Seti Khola, which is unconstrained for the 2012 flood. Given these limitations, our reconstructions of the peak discharge of the May 2012 flood remain first-order estimates, which are likely closer to the upper limit of the potential discharge range. However, our numerical simulations expand on previous empirical assessments of the flood (Kargel et al., 2013; Oi et al., 2014; SANDRP, 2014), which consistently described higher peak discharges (Table 1). Moreover, regression-based estimates of peak discharge from a given dam break may vary by more than an order of magnitude (Walder & Costa, 1996). Our sensitivity analysis for Manning's n in HEC-RAS showed that the model with uniform roughness had a slightly larger flood extent on average (~4%). These differences are more pronounced in areas with for our study area low surface roughness (Manning's $n < 0.08$) such as grassland, bare floodplains or gravel mining sites, consistent with findings from previous work (e.g., Jha & Khare, 2016; Wang et al., 2018; Wohl, 1998). Although these differences seem minute and a varying Manning's n might be less important for larger Q_p scenarios, we argue that roughness may capture important local effects of smaller floods in HEC-RAS simulations. HEC-RAS is sensitive to flow contributions from tributaries as simulated inundation areas of a model including tributary baseflow show mismatches of up to 1.2 km^2 (13%) compared to a simple trunk-channel model with a steady mixed flood of $Q_p = 10{,}000$ m^3 s^{-1}. The greatest mismatches are at the Kali and Phusre Khola confluences. We infer that including the baseflow of tributaries into our geometric model setup provides more realistic flood scenarios.

Our 2D steady-state simulations with ANUGA are a compromise between high computational loads and spatial resolution. We thus had to use a spatially uniform surface roughness and a lower spatial resolution of the triangulated mesh when compared to the original DEM. Modelled flood inundation for $Q_p = 5000$ and $Q_p = 10{,}000$ m^3 s^{-1} agree well with those modelled for 1D flow by HEC-RAS except for mid-reaches containing several gorges, where mean inundation areas differ by a factor of two. Given the model limitations discussed earlier, our peak discharge estimate of 500,000 m^3 s^{-1} for the medieval outburst floods remains a – although physically plausible – speculative first-order assessment. Further, we provide single-event simulations while the number of pulses that deposited the thick sediment beds of the Pokhara Formation remains unknown (Schwanghart et al., 2016). The results of our test of sensitivity of the medieval discharge modelling to the level of valley floor dissection generally agrees with our main findings when routing flow across the modern topography. Although the surface of the Ghachok fan was potentially less incised than today's landscape, outcrops of this formation nevertheless suggest an irregular paleo-topography (Fort, 1987). Thus, our simulations of flow across the modern landscape on the one hand and an idealized smoothed surface on the other hand consider two opposing hypothetical scenarios of the still unknown topography of the Pokhara Valley before the deposition of the Pokhara Formation (Figure 9).

5.2 | The May 2012 and medieval outburst floods in context

Our modelling predicts a peak discharge of the 2012 flood which is roughly half that of prior findings at Kharapani (44%) and Seti dam (53%) (Dwivedi & Neupane, 2013; Kargel et al., 2013; SANDRP, 2014) (Table 1, Figure 10). Published values were derived from hydraulic flow calculations at individual river cross-sections, informed by maximum water stages estimated from video footage or local high-water marks. These divergent Q_p estimates also reflect the different methods and spatial scales of assessment. Our mapping of geomorphic impacts by the May 2012 flood agrees well with reported changes in four channel cross-sections (Gurung et al., 2021), but covers longer reaches of the Seti Khola.

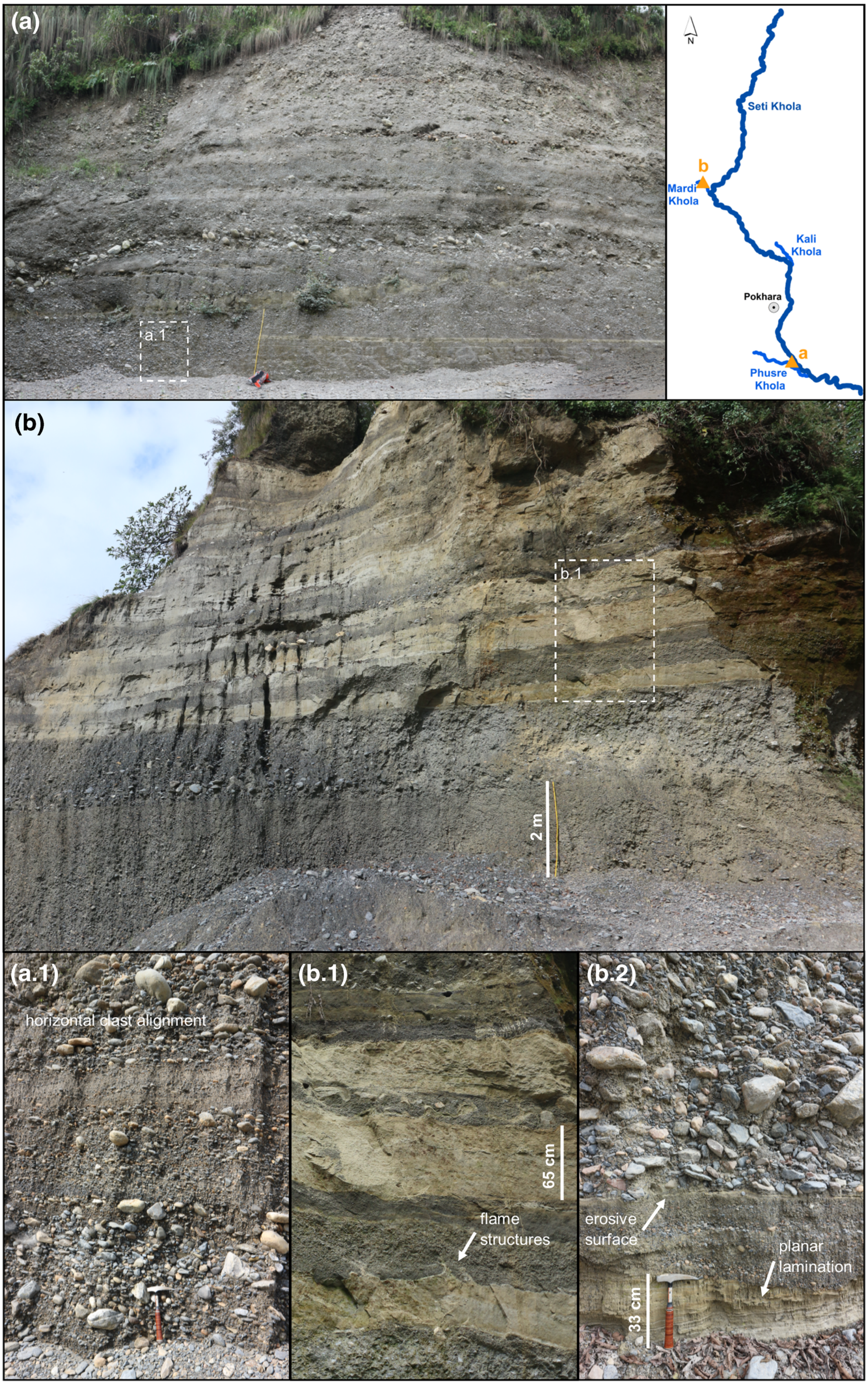

FIGURE 9 Legend on next page.

FIGURE 9 Outcrops of the Pokhara Formation indicating turbulent-flow conditions during deposition. (a) SWS-NEN-orientated road-cut outcrop of Pokhara Formation close to the Phusre Khola confluence. Beds consisting of polymictic, poorly-sorted, matrix-supported breccious conglomerates intercalated with sandier, normal graded beds. (a.1) Distinct horizontal stratification (including horizontal clast alignment). (b) ESE-WNW-orientated road-cut outcrop of Pokhara Formation in the Mardi tributary valley. Two massive beds of polymictic, poorly-sorted, matrix-supported breccious conglomerates showing distinct normal grading in the lower part of the outcrop. Upper part consists of layers of light clay to silts alternating with dark grey coarse sand to granule layers. The coarser layers also contain few lenses of larger cobbles (potential gravel lag). (b.1) Soft-sediment deformation structures (flame structures, load casts) implying rapid deposition of coarser dark material on top of the unconsolidated, water-saturated finer light material. (b.2) Smaller outcrop in *c.* 5 m distance from (b). Planar lamination in predominantly medium sandy material is erosively overlain by a massive bed of breccious conglomerate with partial clast-support and imbrication of longitudinal clasts. [Color figure can be viewed at wileyonlinelibrary.com]

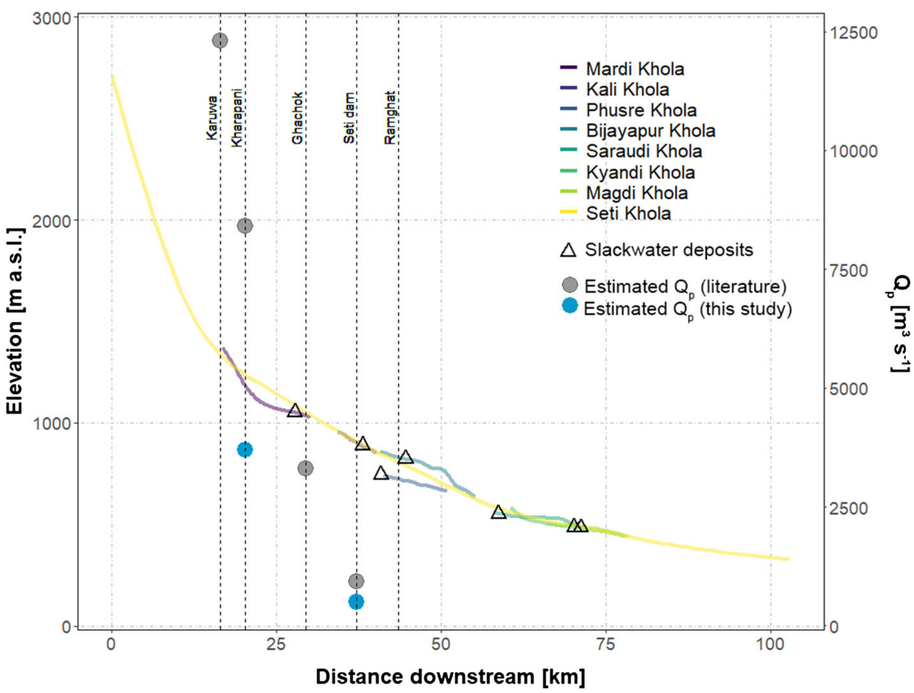

FIGURE 10 Smoothed longitudinal profile of the Seti Khola and its main tributaries. Locations of slackwater deposits in the tributaries are marked by triangles. Points illustrate peak discharge estimates at specific locations. Estimates from previous research are grey (Oi et al., 2012; SANDRP, 2014) and our HEC-RAS-based estimates are blue. [Color figure can be viewed at wileyonlinelibrary.com]

Our estimate of the 2012 peak discharge (Q_p of 3700 $m^3\ s^{-1}$ attenuating to 500 $m^3\ s^{-1}$) is in range of the 100-year flood derived from meteorological flood frequency estimates. Gurung et al. (2021) used HEC-RAS to model local flood stages at two bridges in the upper Seti Khola, and empirically estimated a 100-year flood Q_p of 2420 $m^3\ s^{-1}$ based on local rainfall station data. Basnet et al. (2019) and Basnet & Acharya (2019) simulated peak discharges with HEC-RAS for 10-, 50-, and 100-year floods downstream of the Mardi confluence and Ramghat. While Basnet et al. (2019) also used rainfall station data to estimate the 100-year flood discharge as 1270 $m^3\ s^{-1}$ just downstream of the Mardi confluence, Basnet & Acharya (2019) estimate a discharge of 2340 $m^3\ s^{-1}$ for the 100-year flood at Ramghat based on gauge data from several kilometres downstream of our study area. At Ramghat and Seti Dam, our scenarios of $Q_p = 1000\ m^3\ s^{-1}$ and $Q_p = 2000\ m^3\ s^{-1}$ also yielded comparable results to those by Basnet et al. (2019) and Basnet & Acharya (2019), who used ensembles of HEC-RAS runs, each covering a discrete reach of the Seti Khola exclusive of any gorges.

Our simulations expand on the findings of Basnet et al. (2019), Basnet & Acharya (2019), and Gurung et al. (2021) by highlighting the importance of hydraulic ponding and tributary backwater effects, especially during larger floods ($Q_p > 10{,}000\ m^3\ s^{-1}$). Extensive flooding in all major tributary valleys extends several kilometres upstream when Q_p exceeds 100,000 $m^3\ s^{-1}$ (Figures 7 and 8). The extent of simulated backwater flooding is largely consistent with the location and extent of slackwater deposits laid down during medieval sediment pulses (Schwanghart et al., 2016; Stolle et al., 2017) (Figures 8 and 10). Similar slackwater deposits in other landscapes have been interpreted as evidence of backwater sedimentation during floods (Baker et al., 1983; Carrivick & Rushmer, 2006), for example, for the late Pleistocene Missoula floods (Smith, 1993; Waitt, 1985), or Holocene and historic GLOFs in Patagonia (Benito & Thorndycraft, 2020).

Based on sedimentary evidence, Stolle et al. (2017) argued that catastrophic failure of one or several natural dam(s) potentially following rock-slope failures in the headwaters of the Seti Khola might have generated the medieval sediment pulses that deposited the Pokhara Formation. Our modelling indicates that a large discharge is required to form these deposits, which is consistent with the hypothesis of Stolle et al. (2017). Nonetheless, the spatial coincidence of modelled backwater effects in tributary valleys with the medieval slackwater deposits supports the notion that outburst floods may have shaped the sedimentary record of the Pokhara Valley as tail-ends of earthquake-triggered hazard cascades (Figure 8). Simulated discharges that best fit slackwater deposits slightly exceed field evidence in the upper tributaries, but do not reach them in the lower tributaries. This pattern might hint at multiple medieval outburst flood pulses, during which sediments were deposited first in the upper, and then in the lower, tributary valleys (Schwanghart et al., 2016; Stolle et al., 2017). One exception is the Saraudi Khola, where the inundation modelled on top of the modern topography does not reach the locations of slackwater sediments because of a prominent bedrock knickpoint

2.5 km upstream of the confluence with the Seti Khola (Stolle et al., 2019) (Figure 10). However, our simulations run on the idealized valley floor show that backwater inundation in the Saraudi Khola reaches slackwater sediments for Q_p > 200,000 m^3 s^{-1}. This result further suggests that the fan which the medieval floods crossed was less dissected than the present-day topography. Depositional features of the Pokhara Formation show evidence of rapid sedimentation from bedload-rich, turbulent flow such as stratification and imbrication of clasts, partial clast-support, and normal grading (Figure 9). Stolle et al. (2017) attributed these structures to deposition from highly energetic non-cohesive flows. The necessary amounts of water for such flow conditions could have been provided by the sudden failure of natural dam(s) impounding lake(s) in the Sabche Cirque.

Overall, our outburst flood scenarios in ANUGA cover a wide range of flood peaks, with which we test previous estimates of medieval sediment pulses based on their legacy in the Pokhara Valley (Fort, 2010; Schwanghart et al., 2016). The high magnitude discharge we predict for the medieval outburst floods is comparable to other observed and reconstructed outbursts in High Mountain Asia, such as in the Tsangpo gorge, south-eastern Tibetan Plateau. There, a Q_p of 1.73×10^5 m^3 s^{-1} was generated by the Yigong flood in 2000, whereas Quaternary megafloods from the outburst of an ice-dammed lake generated a Q_p of 5×10^6 m^3 s^{-1} (Turzewski et al., 2019). Our first-order estimate of Q_p of up to 5×10^5 m^3 s^{-1} for the medieval fluvial sediment pulses in Pokhara indicate that floods of this size may have occurred as dam-break hazard cascades at several locations in the Himalayas. The key limitations to peak discharge of lake outbursts are the dam height and the geomorphology of the upstream catchment, which constrain the maximum water volume to be stored in a paleo-lake (Costa & Schuster, 1988). Based on the height of three relict landslide dams in the uppermost Seti Khola gorge and the distinctly steep-walled and bowl-shaped morphology of the Sabche

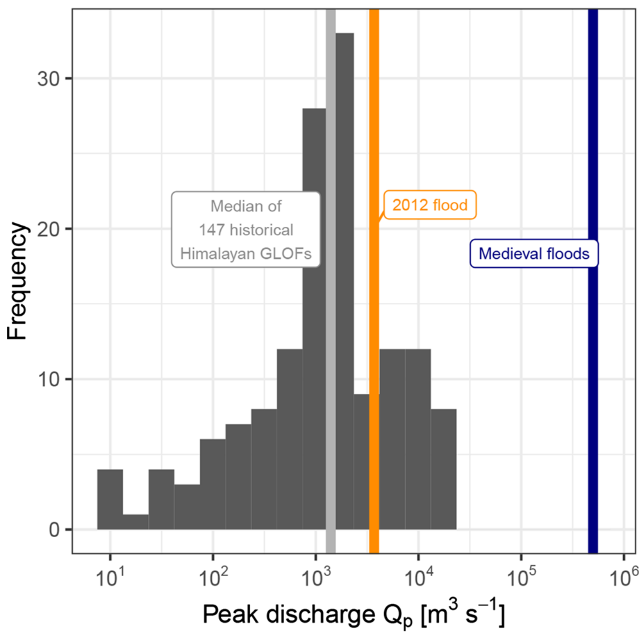

FIGURE 11 Estimated peak discharges of outburst floods in the Pokhara Valley compared to known or reconstructed discharges of glacial lake outburst floods (GLOFs) in the greater Himalayan region derived from Veh et al. (2022). [Color figure can be viewed at wileyonlinelibrary.com]

Cirque, Schwanghart et al. (2016) estimated that former lakes could have stored up to 1 km^3 of meltwater in the headwaters.

The reconstructed discharge of the May 2012 flood is of similar magnitude to reported historic flood discharges, including the Nepalese Dig Tsho GLOF of 1985 (1.6×10^3 m^3 s^{-1} Q_p; Vuichard & Zimmermann, 1987) and the Tam Phokari GLOF of 1998 (1×10^4 m^3 s^{-1} Q_p; Osti & Egashira, 2009) or the flood triggered by the recent 2021 Chamoli rock and ice avalanche, Uttarakhand, India (8–14 $\times 10^3$ m^3 s^{-1}; Shugar et al., 2021) (Figure 11). This latter event was similar to the May 2012 flood along the Seti Khola catchment as it also had a cascading character and propagated along a similarly steep topographic gradient (Gurung et al., 2021; Petley, 2021). The large floodwater and sediment volumes of the Chamoli event were generated by the transformation of a highly mobile ice-rock avalanche into an hyperconcentrated flow; this process has also been discussed as an alternative cause of the 2012 flood in the Seti Khola (Hanisch et al., 2013). These recent hazard cascades impressively illustrated that catastrophic floods with high discharges and sediment fractions can also occur along high-mountain rivers without large water bodies in their headwaters. This observation should be taken into account in hazard and risk assessments for the increasingly densely populated river valleys of the Himalayas.

6 | CONCLUSIONS

We provide new quantitative constraints on the magnitude of catastrophic flooding along the Seti Khola in May 2012 and much larger medieval predecessors. We document channel widening and meander cutting, most pronounced in upper river reaches. The May 2012 flood increased the active channel area by nearly 30% along a 55-km long reach. Using mapped flood sediment as evidence of inundation, we infer that the most likely peak discharge in the upper Seti Khola, where most of the fatalities and damage occurred, was 3700 m^3 s^{-1}. Some 15 km downstream, at the Seti dam in Pokhara city, the estimated, strongly attenuated, discharge is 500 m^3 s^{-1}. We predict peak discharges that are about a factor of two lower than several (empirical) flood estimates reports (Gurung et al., 2015; Oi et al., 2012; SANDRP, 2014).

ANUGA simulations show that extensive backwater effects in the Seti Khola's main tributaries are likely during outburst floods with Q_p > 10,000 m^3 s^{-1}. Modelled backwater flows best match the location of slackwater deposits at a simulated discharge > 500,000 m^3 s^{-1}. Our findings are consistent with the hypothesis that several medieval sediment pulses were likely flood-related and potentially caused by outbursts of meltwater lakes as part of a hazard cascade originating in the Annapurna Massif (Stolle et al., 2017). The simulations of high-magnitude outburst floods also indicate flow expansion and possible channel avulsions, as the alluvial fan in the central Pokhara Valley could be completely inundated by a discharge greater than 300,000 m^3 s^{-1}.

Similar hazards cascades may develop again in the Seti Khola catchment, as unique glaciological and geomorphological conditions in its headwaters may promote outburst floods following glacier surges or rock slope failures. Therefore, planning of regional development in the Pokhara Valley should consider outburst flood hazards, given their repeated historic and potential future impacts and the rising number of people living in close proximity to the Seti Khola.

ACKNOWLEDGEMENTS

This research was funded by the Deutsche Forschungsgemeinschaft (DFG) within the graduate research training group NatRiskChange (GRK 2043/1 and 2043/2) at the University of Potsdam (https://www.natriskchange.de). Karin Lehnigk was supported by a Graduate Research Fellowship from the National Science Foundation (NSF, program-no. 1938059). RapidEye satellite imagery was provided through the Education and Research Program of Planet Lab Inc. (https://www.planet.com/explorer). ALOS WORLD 3D Topographic Data was provided by the Remote Sensing Technology Centre of Japan (©NTT DATA, RESTEC/Included©JAXA). The authors thank Elisabeth Schönfeldt, Monique Fort, and Narayan Gurung for their support in the field. The authors also thank Amelie Stolle for providing the Pokhara Formation outcrop location data. Open Access funding enabled and organized by Projekt DEAL.

CONFLICT OF INTEREST

The authors declare that they have no conflict of interest.

AUTHOR CONTRIBUTIONS

This study was conceptualized by MF, GV, IJL, OK, and AW; MF, GV, and OK carried out the fieldwork. MF, NL, JB, and GV curated the data while MF and KL performed the formal analysis and methodology. MF and GV visualized the data and results. MF prepared the manuscript, KL, GV, IJL, OK, and AW reviewed and edited the writing.

DATA AVAILABILITY STATEMENT

Collected field data was published via the PANGAEA Data Publisher for Earth & Environmental Science (https://www.pangaea.de/) and is available under https://doi.pangaea.de/10.1594/PANGAEA.941540.

ORCID

Melanie Fischer https://orcid.org/0000-0001-7119-7785
Natalie Lützow https://orcid.org/0000-0002-7311-3001

REFERENCES

Arcement Jr, G.J. & Schneider, V.R. (1984) *Guide for selecting Manning's roughness coefficients for natural channels and flood plains: U.S. Geological Survey Water Supply Paper 2339*, US Department of Transportation, Federal Highway Administration.

Baker, V.R., Kochel, R.C., Patton, P.C. & Pickup, G. (1983) *Palaeohydrologic analysis of Holocene flood slack-water sediments*. In: Collision, D. & Lewin, J. (Eds) Modern and Ancient Fluvial Systems: Blackwell SciOxford, Modern and Ancient Fluvial Systems, 229–239. Available from: https://doi.org/10.1002/9781444303773.ch18

Basnet, K. & Acharya, D. (2019) Flood Analysis at Ramghat, Pokhara, Nepal Using HEC-RAS. *Technical Journal*, 1(1), 41–53. Available from: https://doi.org/10.3126/tj.v1i1.27591

Basnet, K., Acharya, D., Bhandari, K.P. & Sadadev, B.B. (2019) *Floodplain Mapping using HEC-RAS (A Case Study of Seti River, Pokhara)*, Pokhara.

Benito, G. & Thorndycraft, V.R. (2020) Catastrophic glacial-lake outburst flooding of the Patagonian ice sheet. *Earth-Science Reviews*, 200(102996), 1–22. Available from: https://doi.org/10.1016/j.earscirev.2019.102996

Blöthe, J.H. & Korup, O. (2013) Millennial lag times in the Himalayan sediment routing system. *Earth and Planetary Science Letters*, 382, 38–46. Available from: https://doi.org/10.1016/j.epsl.2013.08.044

Brunner, G.W. (2020a) *HEC-RAS River Analysis System - Hydraulic Reference Manual*. Washington, D.C.: U.S. Army Corps of Engineers.

Brunner, G.W. (2020b) *HEC-RAS River Analysis System - 2D Modeling User's Manual*. Washington, D.C.: U.S. Army Corps of Engineers.

Burbank, D.W., Blythe, A.E., Putkonen, J., Pratt-Sitaula, B.A., Gabet, E., Oskin, M., et al. (2003) Decoupling of erosion and precipitation in the Himalayas. *Nature*, 426(6967), 652–655. Available from: https://doi.org/10.1038/nature02187

Carrivick, J.L. & Rushmer, E.L. (2006) Understanding high-magnitude outburst floods. *Geology Today*, 22(2), 60–65. Available from: https://doi.org/10.1111/j.1365-2451.2006.00554.x

Carrivick, J.L. (2010) Dam break - outburst flood propagation and transient hydraulics: A geosciences perspective. *Journal of Hydrology*, 380(3–4), 338–355. Available from: https://doi.org/10.1016/j.jhydrol.2009.11.009

Cenderelli, D.A. & Wohl, E.E. (2001) Peak discharge estimates of glacial-lake outburst floods and "normal" climatic floods in the Mount Everest region, Nepal. *Geomorphology*, 40(1–2), 57–90. Available from: https://doi.org/10.1016/S0169-555X(01)00037-X

Cenderelli, D.A. & Wohl, E.E. (2003) Flow hydraulics and geomorphic effects of glacial-lake outburst floods in the Mount Everest region, Nepal. *Earth Surface Processes and Landforms*, 28(4), 385–407. Available from: https://doi.org/10.1002/esp.448

Cesca, M. & D'Agostino, V. (2008) Comparison between FLO-2D and RAMMS in debris-flow modelling: A case study in the Dolomites. *WIT Transactions on Engineering Sciences*, 60, 197–206. Available from: https://doi.org/10.2495/DEB080201

Chen, M., Li, Z., Gao, S., Luo, X., Wing, O.E.J., Shen, X., et al. (2021) A comprehensive flood inundation mapping for hurricane Harvey using an integrated hydrological and hydraulic model. *Journal of Hydrometeorology*, 22(7), 1713–1726. Available from: https://doi.org/10.1175/jhm-d-20-0218.1

Chow, V.T. (1959) *Open-channel hydraulics*, 1st edition. New York: McGraw-Hill.

Costa, J.E. & Schuster, R.L. (1988) The formation and failure of natural dams. *Bulletin Geological Society of America*, 100(7), 1054–1068. Available from: https://doi.org/10.1130/0016-7606(1988)100<1054:TFAFON>2.3.CO;2

Coxon, P., Owen, L.A. & Mitchell, W.A. (1996) A Late Quaternary catastrophic flood in the Lahul Himalayas. *Journal of Quaternary Science*, 11(6), 495–510. Available from: https://doi.org/10.1002/(SICI)1099-1417(199611/12)11:6<495::AID-JQS268>3.0.CO;2-M

Dai, C., Higman, B., Lynett, P.J., Jacquemart, M., Howat, I.M., Liljedahl, A. K., et al. (2020) Detection and assessment of a large and potentially Tsunamigenic periglacial landslide in Barry arm, Alaska. *Geophysical Research Letters*, 47(22), e2020GL089800. Available from: https://doi.org/10.1029/2020GL089800

David, S.R., Larsen, I.J. & Lamb, M.P. (2022) Narrower paleo-canyons downsize Megafloods. *Geophysical Research Letters*, 49(11), e2022GL097861. Available from: https://doi.org/10.1029/2022GL097861

Dussaillant, A., Benito, G., Buytaert, W., Carling, P., Meier, C. & Espinoza, F. (2010) Repeated glacial-lake outburst floods in Patagonia: An increasing hazard? *Natural Hazards*, 54(2), 469–481. Available from: https://doi.org/10.1007/s11069-009-9479-8

Dwivedi, S. & Neupane, Y. (2013) Cause and mechanism of the Seti River flood, 5th may 2012, western Nepal. *Journal of Nepal Geological Society*, 46, 11–18.

Ely, L.L. & Baker, V.R. (1985) Reconstructing Paleoflood hydrology with Slackwater deposits: Verde River, Arizona. *Physical Geography*, 6(2), 103–126. Available from: https://doi.org/10.1080/02723646.1985.10642266

ESRI and Maxar Technologies. (2022) World Imagery [online] Available from: https://services.arcgisonline.com/ArcGIS/rest/services/World_Imagery/MapServer (Accessed 17 May 2022).

Evans, S.G., Bishop, N.F., Smoll, L.F., Murillo, P.V., Delaney, K.B. & Oliver-Smith, A. (2009) A re-examination of the mechanism and human impact of catastrophic mass flows originating on Nevado Huascarán, cordillera Blanca, Peru in 1962 and 1970. *Engineering Geology*, 108(1–2), 96–118. Available from: https://doi.org/10.1016/j.enggeo.2009.06.020

Faeh, R., Mueller, R., Rousselot, P., Veprek, R., Vetsch, D., Volz, C., et al. (2011) *BASEMENT–basic simulation environment for computation of environmental flow and natural Hazard simulation*. Zurich, ETH Zurich.

Fan, X., Xu, Q., Scaringi, G., Dai, L., Li, W., Dong, X., et al. (2017) Failure mechanism and kinematics of the deadly June 24th, 2017 Xinmo landslide, Maoxian, Sichuan, China. *Landslides*, 14(6), 2129–2146. Available from: https://doi.org/10.1007/s10346-017-0907-7

Fort, M. (1987) Sporadic morphogenesis in a continental subduction setting: An example from the Annapurna range, Nepal Himalaya. *Zeitschrift für Geomorphologie Supplementband*, 63, 9–36.

Fort, M. (2010) The Pokhara Valley: A product of a natural catastrophe. In: Migon, P. (Ed.) *Geomorphological landscapes of the World*. Berlin: Springer Springer Dordrecht, pp. 265–274.

Frank, F., McArdell, B.W., Huggel, C. & Vieli, A. (2015) The importance of entrainment and bulking on debris flow runout modeling: Examples from the Swiss Alps. *Natural Hazards and Earth System Sciences*, 15(11), 2569–2583. Available from: https://doi.org/10.5194/nhess-15-2569-2015

Fread, D.L. (1988) *The NWS DAMBRK Model: Quick Users Guide*, Silver Spring: National Weather Service (NWS), NOAA.

George, D.L., Iverson, R.M. & Cannon, C.M. (2017) New methodology for computing tsunami generation by subaerial landslides: Application to the 2015 Tyndall glacier landslide, Alaska. *Geophysical Research Letters*, 44(14), 7276–7284. Available from: https://doi.org/10.1002/2017GL074341

Grandin, R., Doin, M.P., Bollinger, L., Pinel-Puysségur, B., Ducret, G., Jolivet, R., et al. (2012) Long-term growth of the Himalaya inferred from interseismic InSAR measurement. *Geology*, 40(12), 1059–1062. Available from: https://doi.org/10.1130/G33154.1

Gurung, D.R., Maharjan, S.B., Khanal, N.R., Joshi, G. & Murthy, M.S.R. (2015) *Nepal disaster report 2015*. Kathmandu. Kathmandu: Government of Nepal, Ministry of Home Affairs.

Gurung, N., Fort, M., Bell, R., Arnaud-Fassetta, G. & Maharjan, N.R. (2021) Hydro-torrential hazard vs. anthropogenic activities along the Seti valley, Kaski, Nepal: Assessment and recommendations from a risk perspective. *Journal of Nepal Geological Society*, 62, 58–87. Available from: https://doi.org/10.3126/jngs.v62i0.38695

Haeberli, W. & Whiteman, C. (2021) Snow and ice-related hazards, risks, and disasters: Facing challenges of rapid change and long-term commitments. In: Haeberli, W. & Whiteman, C. (Eds.) *Snow and ice-related hazards, risks, and disasters*. Amsterdam, Oxford, Cambridge: Elsevier pp. 1–33. Available from: https://doi.org/10.1016/B978-0-12-817129-5.00014-7

Hanisch, J., Koirala, A. & Bhandary, N.P. (2013) The Pokhara may 5th flood disaster: A last warning sign sent by nature? *Journal of Nepal Geological Society*, 46, 1–10.

Hauser, A. (2002) Rock avalanche and resulting debris flow in Estero Parraguirre and Rio Colorado, Region Metropolitana, Chile. In: Evans, S.G. & DeGraff, J.V. (Eds.) *Catastrophic landslides: Effects, occurrence and mechanisms*, Vol. 15. Boulder: Geological Society of America Reviews in Engineering Geology, pp. 135–148.

Hock, R., Rasul, G., Adler, C., Cáceres, B., Gruber, S., Hirabayashi, Y., et al. (2019) I.: High Mountain Areas. In: Pörtner, H.-O., Roberts, D.C., Masson-Delmotte, V., Zhai, P., Tignor, M., Poloczanska, E., et al. (Eds.) *IPCC special report on the ocean and cryosphere in a changing climate*. Genf: Intergovernmental Panel on Climate Change (IPCC), pp. 131–202. Available from: https://doi.org/10.1017/9781009157964.004

Hormann, K. (1974) Die Terrassen an der Seti Khola - Ein Beitrag zur quartären Morphogenese in Zentralnepal. *Erdkunde*, 28(3), 161–176.

Huang, D., Li, Y.Q., Song, Y.X., Xu, Q. & Pei, X.J. (2019) Insights into the catastrophic Xinmo rock avalanche in Maoxian county, China: Combined effects of historical earthquakes and landslide amplification. *Engineering Geology*, 258, 105–158. Available from: https://doi.org/10.1016/j.enggeo.2019.105158

Huber, M.L., Lupker, M., Gallen, S.F., Christl, M. & Gajurel, A.P. (2020) Timing of exotic, far-traveled boulder emplacement and paleo-outburst flooding in the Central Himalayas. *Earth Surface Dynamics*, 8(3), 769–787. Available from: https://doi.org/10.5194/esurf-8-769-2020

Jacquemart, M., Loso, M., Leopold, M., Welty, E., Berthier, E., Hansen, J. S.S., et al. (2020) What drives large-scale glacier detachments? Insights from Flat Creek glacier, St. Elias mountains, Alaska. *Geology*, 48(7), 703–707. Available from: https://doi.org/10.1130/G47211.1

Jha, L.K. & Khare, D. (2016) Glacial lake outburst flood (GLOF) study of Dhauliganga basin in the Himalaya. *Cogent Environmental Science*, 2(1), 1–13. Available from: https://doi.org/10.1080/23311843.2016.1249107

Kargel, J.S., Paudel, L., Leonard, G., Regmi, D., Joshi, S., Poudel, K., et al. (2013) Causes and human impacts of the Seti River (Nepal) disaster of 2012. In: *Glacial Flooding & Disaster Risk Management Knowledge Exchange and field training*. Huaraz, Peru: High Mountains Adaptation Partnership, pp. 1–11, Huaraz.

Klimeš, J., Benešová, M., Vilímek, V., Bouška, P. & Cochachin Rapre, A. (2014) The reconstruction of a glacial lake outburst flood using HEC-RAS and its significance for future hazard assessments: An example from Lake 513 in the cordillera Blanca, Peru. *Natural Hazards*, 71(3), 1617–1638. Available from: https://doi.org/10.1007/s11069-013-0968-4

Korup, O. & Montgomery, D.R. (2008) Tibetan plateau river incision inhibited by glacial stabilization of the Tsangpo gorge. *Nature*, 455(7214), 786–789. Available from: https://doi.org/10.1038/nature07322

Larsen, I.J. & Lamb, M.P. (2016) Progressive incision of the channeled scablands by outburst floods. *Nature*, 538(7624), 229–232. Available from: https://doi.org/10.1038/nature19817

Lehnigk, K.E. & Larsen, I.J. (2022) Pleistocene Megaflood discharge in grand coulee, channeled scabland, USA. *Journal of Geophysical Research - Earth Surface*, 127(1), 1–25. Available from: https://doi.org/10.1029/2021JF006135

Mergili, M., Fischer, J.T., Krenn, J. & Pudasaini, S.P. (2017) R.avaflow v1, an advanced open-source computational framework for the propagation and interaction of two-phase mass flows. *Geoscientific Model Development*, 10(2), 553–569. Available from: https://doi.org/10.5194/gmd-10-553-2017

Mergili, M., Schneider, D., Worni, R. & Schneider, J.F. (2011) Glacial lake outburst floods in the Pamir of Tajikistan: Challenges in prediction and modelling, Int. Conf. Debris-Flow Hazards Mitig. Mech. Predict. Assessment, Proc. Available from: https://doi.org/10.4408/IJEGE.2011-03.B-106

Mungkasi, S., van Drie, R. & Roberts, S.G. (2013) Predictions on arrival times of water of the St. Francis dam break flood using ANUGA. In Proceedings - 20th International Congress on Modelling and Simulation (MODSIM 2013), pp. 304–309, Adelaide.

O'Brien, J.S., Julien, P.Y. & Fullerton, W.T. (1993) Two-dimensional water flood and mudflow simulation. *Journal of Hydraulic Engineering*, 119(2), 244–261. Available from: https://doi.org/10.1061/(ASCE)0733-9429(1993)119:2(244)

Oi, H., Higaki, D., Yagi, H., Usuki, N. & Yoshino, K. (2012) *Survey report on the Seti River flood, Nepal (May 5, 2012)*. Tokyo: Sabo Frontier Foundation.

Oi, H., Higaki, D., Yagi, H., Usuki, N. & Yoshino, K. (2014) Report of the investigation of the flood disaster that occurred on may 5, 2012 along the Seti River in Nepal. *International Journal of Erosion Control Engineering*, 7(4), 111–117. Available from: https://doi.org/10.13101/ijece.7.111

Osti, R. & Egashira, S. (2009) Hydrodynamic characteristics of the tam Pokhari glacial lake outburst flood in the Mt. Everest region, Nepal. *Hydrological Processes*, 23(20), 2943–2955. Available from: https://doi.org/10.1002/hyp.7405

Petley, D. (2021) The catastrophic landslide and flood in Chamoli in Uttarakhand: the sequence of events, Landslide Blog - AGU Blogosph. [online] Available from: https://blogs.agu.org/landslideblog/2021/02/08/chamoli-2/ (Accessed 16 July 2021).

Planet Team. (2017) Planet Application Program Interface: In Space for Life on Earth, [online] Available from: https://www.planet.com/explorer (Accessed 17 May 2022).

Richardson, S.D. & Reynolds, J.M. (2000) An overview of glacial hazards in the Himalayas. *Quaternary International*, 65(66), 31–47. Available from: https://doi.org/10.1016/S1040-6182(99)00035-X

Rimal, B. (2012) Urbanization and the decline of agricultural land in Pokhara Sub-Metropolitan City, Nepal. *The Journal of Agricultural Science*, 5(1), 54–65. Available from: https://doi.org/10.5539/jas.v5n1p54

Rimal, B., Baral, H., Stork, N., Paudyal, K. & Rijal, S. (2015) Growing City and rapid land use transition: Assessing multiple hazards and risks in the Pokhara Valley, Nepal. *Land*, 4(4), 957–978. Available from: https://doi.org/10.3390/land4040957

Rimal, B., Zhang, L., Keshtkar, H., Sun, X. & Rijal, S. (2018) Quantifying the spatiotemporal pattern of urban expansion and hazard and risk area identification in the Kaski District of Nepal. *Land*, 7(37), 1–22. Available from: https://doi.org/10.3390/land7010037

Roberts, S., Nielsen, O., Gray, D. & Sexton, J. (2015) *ANUGA User Manual*. Symonstron: Geoscience Australia. Available from: https://doi.org/10.13140/RG.2.2.12401.99686

Ross, J. & Gilbert, R. (1999) Lacustrine sedimentation in a monsoon environment: The record from Phewa Tal, middle mountain region of Nepal. *Geomorphology*, 27(3–4), 307–323. Available from: https://doi.org/10.1016/S0169-555X(98)00079-8

SANDRP. (2014) Explained: Seti River floods in May 2012, Nepal- A chain of events, starting at 25,000 feet!, [online] Available from: https://sandrp.in/2014/01/26/explained-seti-river-floods-in-may-2012-nepal-a-chain-of-events-starting-at-25000-feet/ (Accessed 18 March 2021).

Sattar, A., Haritashya, U.K., Kargel, J.S., Leonard, G.J., Shugar, D.H. & Chase, D.V. (2021) Modeling Lake outburst and downstream hazard assessment of the lower Barun glacial lake, Nepal Himalaya. *Journal of Hydrology*, 598, 126208. Available from: https://doi.org/10.1016/j.jhydrol.2021.126208

Schwanghart, W., Bernhardt, A., Stolle, A., Hoelzmann, P., Adhikari, B.R., Andermann, C., et al. (2016) Repeated catastrophic valley infill following medieval earthquakes in the Nepal Himalaya. *Science*, 351(6269), 147–150. Available from: https://doi.org/10.1126/science.aac9865

Shang, Y., Yang, Z., Li, L., Liu, D., Liao, Q. & Wang, Y. (2003) A super-large landslide in Tibet in 2000: Background, occurrence, disaster, and origin. *Geomorphology*, 54(3–4), 225–243. Available from: https://doi.org/10.1016/S0169-555X(02)00358-6

Shugar, D.H., Jacquemart, M., Shean, D., Bhushan, S., Upadhyay, K., Sattar, A., et al. (2021) A massive rock and ice avalanche caused the 2021 disaster at Chamoli, Indian Himalaya. *Science*, 373(6552), 300–306. Available from: https://doi.org/10.1126/science.abh4455

Smith, G.A. (1993) Missoula flood dynamics and magnitudes inferred from sedimentology of slack-water deposits on the Columbia plateau, Washington. *Geological Society of America Bulletin*, 105(1), 77–100. Available from: https://doi.org/10.1130/0016-7606(1993)105<0077:MFDAMI>2.3.CO;2

Somos-Valenzuela, M.A., McKinney, D.C., Byers, A.C., Rounce, D.R., Portocarrero, C. & Lamsal, D. (2014) Assessing downstream flood impacts due to a potential GLOF from Imja Lake in Nepal. *Hydrology and Earth System Sciences Discussions*, 11(11), 13019–13053. Available from: https://doi.org/10.5194/hessd-11-13019-2014

Srivastava, P., Kumar, A., Chaudhary, S., Meena, N., Sundriyal, Y.P., Rawat, S., et al. (2017) Paleofloods records in Himalaya. *Geomorphology*, 284, 17–30. Available from: https://doi.org/10.1016/j.geomorph.2016.12.011

Stolle, A., Bernhardt, A., Schwanghart, W., Hoelzmann, P., Adhikari, B.R., Fort, M., et al. (2017) Catastrophic valley fills record large Himalayan earthquakes, Pokhara, Nepal. *Quaternary Science Reviews*, 177, 88–103. Available from: https://doi.org/10.1016/j.quascirev.2017.10.015

Stolle, A., Schwanghart, W., Andermann, C., Bernhardt, A., Fort, M., Jansen, J.D., et al. (2019) Protracted river response to medieval earthquakes. *Earth Surface Processes and Landforms*, 44(1), 331–341. Available from: https://doi.org/10.1002/esp.4517

Toonen, W.H.J., Munoz, S.E., Cohen, K.M. & Macklin, M.G. (2020) High-Resolution Sedimentary Paleoflood Records in Alluvial River Environments: A Review of Recent Methodological Advances and Application to Flood Hazard Assessment. In: Herget, J. & Fontana, A. (Eds.) *Palaeohydrology: Traces, tracks and trails of extreme events*. Cham: Springer International Publishing, pp. 213–228.

Turzewski, M.D., Huntington, K.W. & LeVeque, R.J. (2019) The geomorphic impact of outburst floods: Integrating observations and numerical simulations of the 2000 Yigong flood, eastern Himalaya. *Journal of Geophysical Research - Earth Surface*, 124(5), 1056–1079. Available from: https://doi.org/10.1029/2018JF004778

Veh, G., Lützow, N., Kharlamova, V., Petrakov, D., Hugonnet, R. & Korup, O. (2022) Trends, breaks, and biases in the frequency of reported glacier Lake outburst floods. *Earth's Future*, 10(3), 1–14. Available from: https://doi.org/10.1029/2021EF002426

Vuichard, D. & Zimmermann, M. (1987) The 1985 catastrophic drainage of a moraine-dammed lake, Khumbu Himal, Nepal: Cause and consequences. *Mountain Research and Development*, 7(2), 91–110. Available from: https://doi.org/10.2307/3673305

Waitt, R.B. (1985) Case for periodic, colossal jokulhlaups from Pleistocene glacial Lake Missoula. *Geological Society of America Bulletin*, 96(10), 1271–1286. Available from: https://doi.org/10.1130/0016-7606(1985)96<1271:CFPCJF>2.0.CO;2

Walder, J.S. & Costa, J.E. (1996) Outburst floods from glacier-Dammed Lakes: The effect of mode of Lake drainage on flood magnitude. *Earth Surface Processes and Landforms*, 21(8), 701–723. Available from: https://doi.org/10.1002/(SICI)1096-9837(199608)21:8<701::AID-ESP615>3.0.CO;2-2

Wang, W., Gao, Y., Iribarren Anacona, P., Lei, Y., Xiang, Y., Zhang, G., et al. (2018) Integrated hazard assessment of Cirenmaco glacial lake in Zhangzangbo valley, Central Himalayas. *Geomorphology*, 306, 292–305. Available from: https://doi.org/10.1016/j.geomorph.2015.08.013

Wang, W., Yang, X. & Yao, T. (2012) Evaluation of ASTER GDEM and SRTM and their suitability in hydraulic modelling of a glacial lake outburst flood in Southeast Tibet. *Hydrological Processes*, 26(2), 213–225. Available from: https://doi.org/10.1002/hyp.8127

Westoby, M.J., Glasser, N.F., Brasington, J., Hambrey, M.J., Quincey, D.J. & Reynolds, J.M. (2014) Modelling outburst floods from moraine-dammed glacial lakes. *Earth-Science Reviews*, 134, 137–159. Available from: https://doi.org/10.1016/j.earscirev.2014.03.009

Wilhelm, B., Ballesteros Canovas, J.A., Corella Aznar, J.P., Kämpf, L., Swierczynski, T., Stoffel, M., et al. (2018) Recent advances in paleoflood hydrology: From new archives to data compilation and analysis. *Water Security*, 3, 1–8. Available from: https://doi.org/10.1016/j.wasec.2018.07.001

Wohl, E.E. (1995) Estimating flood magnitude in ungauged mountain channels, Nepal. *Mountain Research and Development*, 15(1), 69–76. Available from: https://doi.org/10.2307/3673701

Wohl, E.E. (1998) Uncertainty in flood estimates associated with roughness coefficient. *Journal of Hydraulic Engineering*, 124(2), 219–223. Available from: https://doi.org/10.1061/(asce)0733-9429(1998)124:2(219)

Worni, R., Huggel, C., Clague, J.J., Schaub, Y. & Stoffel, M. (2014) Coupling glacial lake impact, dam breach, and flood processes: A modeling perspective. *Geomorphology*, 224, 161–176. Available from: https://doi.org/10.1016/j.geomorph.2014.06.031

Zhang, X. & Liu, S. (2015) A framework of numerical simulation on moraine-dammed glacial lake outburst floods. *Journal of Arid Land*, 7(6), 728–740. Available from: https://doi.org/10.1007/s40333-015-0133-x

SUPPORTING INFORMATION

Additional supporting information can be found online in the Supporting Information section at the end of this article.

How to cite this article: Fischer, M., Lehnigk, K., Lützow, N., Brettin, J., Veh, G., Larsen, I.J. et al. (2023) Himalayan hazard cascades – modern and medieval outburst floods in Pokhara, Nepal. *Earth Surface Processes and Landforms*, 48(6), 1135–1151. Available from: https://doi.org/10.1002/esp.5539